Relative Importance of High-Latitude Local and Long-Range Transported Dust to Arctic Ice Nucleating Particles and Impacts on Arctic Mixed-Phase Clouds

Yang Shi[1], Xiaohong Liu[1], Mingxuan Wu[2], Xi Zhao[1], Ziming Ke[1], and Hunter Brown[1]

[1]Department of Atmospheric Sciences, Texas A&M University, College Station, TX, USA
[2]Atmospheric Sciences and Global Change Division, Pacific Northwest National Laboratory, Richland, WA, USA

Correspondence to: Xiaohong Liu (xiaohong.liu@tamu.edu)

Abstract. Dust particles, serving as ice nucleating particles (INPs), may impact the Arctic surface energy budget and regional climate by modulating the mixed-phase cloud properties and lifetime. In addition to long-range transport from low latitude deserts, dust particles in the Arctic can originate from local sources. However, the importance of high latitude dust (HLD) as a source of Arctic INPs (compared to low latitude dust (LLD)) and its effects on Arctic mixed-phase clouds are overlooked. In this study, we evaluate the contribution to Arctic dust loading and INP population from HLD and six LLD source regions by implementing a source-tagging technique for dust aerosols in version 1 of the US Department of Energy's Energy Exascale Earth System Model (E3SMv1). Our results show that HLD is responsible for 30.7% of the total dust burden in the Arctic, whereas LLD from Asia and North Africa contribute 44.2% and 24.2%, respectively. Due to its limited vertical transport as a result of stable boundary layers, HLD contributes more in the lower troposphere, especially in boreal summer and autumn when the HLD emissions are stronger. LLD from North Africa and East Asia dominates the dust loading in the upper troposphere with peak contributions in boreal spring and winter. The modeled INP concentrations show a better agreement with both ground and aircraft INP measurements in the Arctic when including HLD INPs. The HLD INPs are found to induce a net cooling effect (-0.24 W m^{-2} above 60°N) on the Arctic surface downwelling radiative flux by changing the cloud phase of the Arctic mixed-phase clouds. The magnitude of this cooling is larger than those induced by North African and East Asian dust (0.08 and -0.06 W m^{-2}, respectively), mainly due to different seasonalities of HLD and LLD. Uncertainties of this study are discussed, which highlights the importance of further constraining the HLD emissions.

1 Introduction

The Arctic has experienced long-term climate changes, including rapid warming and shrinking in sea ice extent. Arctic mixed-phase clouds (AMPCs), which occur frequently throughout the year, strongly impact the surface and atmospheric energy budget and are one of the main components driving the Arctic climate (Morrison et al., 2012; Shupe and Intrieri, 2004; Tan and Storelvmo, 2019). The AMPCs lifetime, properties, and radiative effects are closely connected to the primary ice formation process, as the formed ice crystals grow at the expense of cloud liquid droplets due to the lower saturation vapor pressure with respect to ice than that to liquid water (so-called Wegener-Bergeron-Findeisen process or, in short, WBF process; Liu et al., 2011; M. Zhang et al., 2019). Large ice crystals with higher fall speeds than liquid droplets can readily initiate precipitation and further deplete cloud liquid through the riming process. All these processes can also interact with each other nonlinearly and impact the phase partitioning of mixed-phase clouds (Tan and Storelvmo, 2016).

Primary ice formation in mixed-phase clouds only occurs heterogeneously with the aid of ice nucleating particles (INPs). According to Vali et al. (1985), the heterogeneous ice nucleation is classified into four different modes: through the collision of an INP particle with supercool liquid droplet (contact freezing), by an INP particle immersed in a liquid droplet (immersion freezing), when the INP particle also serves as a cloud condensation nucleus (condensation freezing), or by the direct deposition of water vapor to a dry INP particle (deposition nucleation). The immersion freezing is usually treated together with condensation freezing in models, as instruments cannot distinguish between them (Vali et al., 2015). This immersion/condensation freezing is generally thought to be the most important ice nucleation mode in the mixed-phase clouds (de Boer et al., 2011; Prenni et al., 2009; Westbrook and Illingworth, 2013). It remains a significant challenge to

56 characterize the INP types and concentrations, partially because only a very small fraction of

57 aerosols can serve as INPs (DeMott et al., 2010). This is especially the case for the clean

58 environment in the Arctic. Therefore, the potential sources and amounts of Arctic INPs are still

59 largely unknown.

60 Mineral dust aerosols are identified as one of the most important types of INPs in the

61 atmosphere due to their high ice nucleation efficiency (DeMott et al., 2003; Hoose and Möhler,

62 2012; Murray et al., 2012; Atkinson et al., 2013) and their abundance in the atmosphere (Kinne

63 et al., 2006). They are mainly emitted from arid and semi-arid regions located at low- to mid-

64 latitudes, such as North Africa, the Middle East, and Asia. Observational studies found that LLD

65 can be transported to the Arctic (Bory et al., 2003; VanCuren et al., 2012; Huang et al., 2015)

66 and act as a key contributor to the Arctic INP population (Si et al., 2019). A modelling study also

67 suggested that low latitude dust (LLD) has a large contribution to dust concentrations in the

68 upper troposphere of the Arctic (Groot Zwaaftink et al., 2016), since LLD is usually lifted by

69 convection and topography and then transported poleward following slantwise isentropes. This

70 finding confirms the potential of LLD to serve as INPs in AMPCs. The impact of LLD INPs on

71 clouds was further investigated by Shi and Liu (2019), who found that LLD INPs induce a net

72 cooling cloud radiative effect in the Arctic, due to their impacts on cloud water path and cloud

73 fraction.

74 Although LLD has attracted much of the attention in the past, it is recognized that 2–3% of the

75 global dust emission is produced by local Arctic sources above 50°N (Bullard et al., 2016),

76 which include Iceland (Arnalds et al., 2016; Dagsson-Waldhauserova et al., 2014; Prospero et al.,

77 2012), Svalbard (Dörnbrack et al., 2010), Alaska (Crusius et al., 2011), and Greenland (Bullard

78 and Austin, 2011). Groot Zwaaftink et al. (2016) found that high latitude dust (HLD) contributes

79 27% of the total dust burden in the Arctic. Different from LLD, most of the emitted HLD is

80 restricted at the lower altitudes in the Arctic, because of the stratified atmosphere in the cold

81 environment (Bullard, 2017; Groot Zwaaftink et al., 2016).

82   It is also noted that HLD is likely an important source to the observed INPs in the Arctic,

83 especially during the warm seasons. For example, Irish et al. (2019) suggested that mineral dust

84 from Arctic bare lands (likely eastern Greenland or north-western continental Canada) is an

85 important contributor to the INP population in the Canadian Arctic marine boundary layer during

86 summer 2014. Attempts have been made to quantify the ice nucleating ability of HLD.

87 Paramonov et al. (2018) found that the Icelandic glaciogenic silt had a similar ice nucleating

88 ability as LLD at temperatures below -30 °C. Similarly, Sanchez-Marroquin et al. (2020)

89 suggested that the ice nucleating ability of aircraft-collected Icelandic dust samples is slightly

90 lower but comparable with that of the LLD. Some other studies also noticed that HLD can act as

91 efficient INPs at warm temperatures. As early as the 1950s, the airborne dry dust particles from

92 permafrost ground at Thule, Greenland, were found to nucleate ice at temperatures as warm as -5

93 °C (Fenn and Weickmann, 1959). This is corroborated by a more recent study which investigated

94 the glacial outwash sediments in Svalbard and ascribed the remarkably high ice nucleating

95 ability to the presence of soil organic matter (Tobo et al., 2019).

96   Despite their potential importance, HLD sources are largely underestimated or even omitted in

97 global models (Zender et al., 2003). Fan (2013) noticed that the autumn peak in measured

98 surface dust concentrations at Alert was underestimated by the model, likely due to a lack of

99 local dust emission. Similarly, Shi and Liu (2019) also mentioned that the distinction of

100 simulated and satellite retrieved dust vertical extinction in the Arctic became larger near the

101 surface.

102   In this study, we account for the HLD dust emission by replacing the default dust emission

103   scheme (Zender et al., 2003) with the Kok et al. (2014a, b) scheme in the Energy Exascale Earth

104   System Model version 1 (E3SMv1). We further track explicitly the dust aerosols emitted from

105   the Arctic (HLD) and six major LLD sources using a newly developed source-tagging technique

106   in E3SMv1. The objectives of this study are to (1) examine the source attribution of the Arctic

107   dust aerosols in the planetary boundary layer and in the free troposphere; (2) examine the

108   contribution of dust from various sources to the Arctic dust INPs; and (3) quantify the

109   subsequent influence of dust INPs from various sources on the Arctic mixed-phase cloud

110   radiative effects. We are particularly interested in the relative importance of local HLD versus

111   long-range transported LLD.

112   The paper is organized as follows. The E3SMv1 model and experiments setup are introduced

113   in Section 2. Section 3 presents model results and comparisons with observations. The

114   uncertainties are discussed in Section 4, and Section 5 summarizes the results.

115   **2 Methods**

116   **2.1 Model description and experiment setup**

117   Experiments in this study are performed using the atmosphere component (EAMv1) of the U.S.

118   Department of Energy (DOE) E3SMv1 model (Rasch et al., 2019). The model predicts number

119   and mass mixing ratios of seven aerosol species (i.e., mineral dust, black carbon (BC), primary

120   organic aerosol, secondary organic aerosol, sulfate, sea salt, and marine organic aerosol (MOA))

121   through a four-mode version of modal aerosol module (MAM4) (Liu et al., 2016; Wang et al.,

122   2020). The four aerosol modes are Aitken, accumulation, coarse, and primary-carbon modes,

123   while dust aerosols are carried in accumulation and coarse modes. Aerosol optical properties in

124   each mode is parameterized following Ghan and Zaveri (2007). The dust optics used in this study

125   are updated according to Albani et al. (2014).

126   EAMv1 includes a two-moment stratiform cloud microphysics scheme (MG2) (Gettelman and

127   Morrison, 2015). We note the WBF process rate in EAMv1 is tuned down by a factor of 10,

128   which results in more prevalent supercooled liquid water clouds in high latitudes than

129   observations and many other global climate models (Y. Zhang et al., 2019; Zhang et al., 2020).

130   In addition, the Cloud Layers Unified By Binormals (CLUBB) parameterization (Bogenschutz et

131   al., 2013; Golaz and Larson, 2002; Larson et al., 2002) is used to unify the treatments of

132   planetary boundary layer turbulence, shallow convection, and cloud macrophysics. Deep

133   convection is treated by the Zhang and McFarlane (1995) scheme.

134   In EAMv1, the heterogeneous ice nucleation in mixed-phase clouds follows the classical

135   nucleation theory (CNT) (Hoose et al., 2010; Y. Wang et al., 2014). CNT holds the stochastic

136   hypothesis, which treats the ice nucleation process as a function of time.

137   Immersion/condensation, contact, and deposition nucleation on dust and BC are treated in the

138   CNT scheme. More details about CNT parameterization are provided in Text S2.1 in the

139   Supplement.

140   The experiments we conducted for this study are shown in Table 1. For the control experiment

141   (hereafter CTRL), the EAMv1 was integrated from July 2006 to the end of 2011 at 1° horizontal

142   resolution and 72 vertical layers. The first six months of the experiment were treated as model

143   spin-up and the last five-year results were used in analyses. The horizontal wind components

144   were nudged to the MERRA2 meteorology with a relaxation timescale of 6 hours (Zhang et al.,

145   2014). In addition to CTRL, we conducted three sensitivity experiments to investigate the INP

146   effect of dust from major source regions. In these sensitivity experiments, heterogeneous ice

147   nucleation in the mixed-phase clouds by dust from local Arctic sources, North Africa, and East

148   Asia is turned off (i.e., noArc, noNAf, and noEAs, respectively). The other settings of these three

149   experiments are identical to CTRL. Analyses related to the sensitivity experiments are provided

150   in Section 3.4.

151   **2.2 Dust emission parameterization and source-tagging technique**

152   Dust emission in the default EAMv1 is parameterized following Zender et al. (2003) (Z03),

153   which uses semi-empirical dust source functions to address the spatial variability in soil

154   erodibility. The HLD emission is omitted in the Z03 scheme, since it was thought to be dubious

155   (Zender et al., 2003). In this study, we replaced the Z03 scheme with another dust emission

156   parameterization (Kok et al., 2014a, b) (K14) that avoids using a source function (see more

157   details about K14 in Text S1). The K14 scheme is able to produce the HLD emission over

158   Iceland, the Greenland coast, Canada, Svalbard, and North Eurasia (Figure 1a). Furthermore, to

159   address the overestimation in dust emission in clay size ($< 2~\mu$m diameter) (Kok et al., 2017), we

160   changed the size distribution of emitted dust particles from Z03 to that based on the brittle

161   fragmentation theory (Kok, 2011). 1.1% of the total dust mass is emitted to the accumulation

162   mode and 98.9% of that is emitted to the coarse mode based on the brittle fragmentation theory,

163   whereas the fractions are 3.2% and 96.8%, respectively in Z03.

164   To quantify the source attribution of dust, we implemented a dust source-tagging technique in

165   EAMv1. This modeling tool was previously applied to BC (H. Wang et al., 2014; Yang et al.,

166   2017b), sulfate (Yang et al., 2017a), and primary organic aerosol (Yang et al., 2018) in the

167   Community Atmosphere Model version 5 (CAM5). In this method, dust emission fluxes from

168   different sources are assigned to separate tracers and transport independently, so that dust

169   originating from different sources can be tracked and tuned separately in a single model

170   experiment. As shown in Figure 1a, dust emissions from 7 source regions are tagged: Arctic (Arc;

171   above 60°N, HLD source), North America (NAm), North Africa (NAf), Central Asia (CAs),

172   Middle East and South Asia (MSA), East Asia (EAs), and rest of the world (RoW). The Arctic

173   source is further divided into four sub-sources: Alaska (Ala), North Canada (NCa), Greenland

174   and Iceland (GrI), and North Eurasia (NEu) (Figure S1), which are used in the analysis of INP

175   sources in Section 3.3. RoW represents the three major dust sources in the Southern Hemisphere

176   (South America, South Africa, and Australia), along with very low emissions from Europe and

177   the Antarctic.

178   The global dust emission for CTRL is 5640 Tg yr^{-1}, which is tuned so that the global average

179   dust aerosol optical depth (DOD) is 0.031. This is within the range of the observational estimate

180   (0.030±0.005) by Ridley et al. (2016). To maintain the magnitude of the global averaged DOD,

181   our tuned global dust emission exceeds the range of the AeroCom (Aerosol Comparisons

182   between Observations and Models) models (500 to 4400 Tg yr^{-1}; Huneeus et al., 2011), likely

183   due to a short lifetime caused by too strong dust dry deposition at the bottom layer near the dust

184   source regions in EAMv1 (Wu et al., 2020). It is also about 2000 Tg yr^{-1} higher than the previous

185   EAMv1 studies (Shi and Liu, 2019; Wu et al., 2020), because we distribute less dust mass into

186   the accumulation mode and more dust mass into the coarse mode based on Kok (2011). The

187   HLD emission is further tuned up by 10 times so that it accounts for 2.6% (144 Tg yr^{-1}) of the

188   global dust emission (Figure 1b), which is comparable with the recent estimates of 2-3% above

189   50°N by Bullard et al. (2016) and of 3% above 60°N by Groot Zwaaftink et al. (2016). The

190   majority of global dust emission is contributed from North Africa (51.9%, 2929 Tg yr^{-1}) and

191   Asia (37.7%, 2124 Tg yr^{-1}), with Asian emissions composed of MSA (20.2%, 1140 Tg yr^{-1}), EAs

192   (10.9%, 613 Tg yr^{-1}), and CAs (6.6%, 371 Tg yr^{-1}). NAm has a weak dust emission of 33.4 Tg

193 yr^{-1} that only contributes 0.6% to the global emission, while the RoW has a combined

194 contribution of 7.3% (410 Tg yr^{-1}). In addition, the seasonal variations between HLD and LLD

195 emissions are different - the HLD (Arctic) source is more active in late summer and autumn,

196 while the LLD sources (e.g., NAf, MSA, EAs) peak in spring and early summer (Figure 1c).

3 Result

3.1 Model validation

199 To evaluate the model performance in simulating the dust cycle, we compare the model

200 predictions with measured aerosol optical depth (AOD), dust surface concentrations, and dust

201 deposition fluxes from global observation networks (Figure 2). We select and process the level

202 2.0 AOD data (2007-2011) at 40 "dust-dominated" AErosol RObotic NETwork (AERONET;

203 Holben et al., 1998) stations following Kok et al. (2014b). We note that the AERONET AOD

204 measurements are biased towards clear-sky conditions due to the cloud-screening procedure

205 (Smirnov et al., 2000). For dust surface concentrations, we use the same measurements at 22

206 sites, which Huneeus et al. (2011) used for the AeroCom comparison, and further extend the

207 dataset with measurements at three high latitude stations: Heimaey (Prospero et al., 2012), Alert

208 (Sirois and Barrie, 1999), and Trapper Creek (Interagency Monitoring of Protected Visual

209 Environments; IMPROVE). It is noted that the measurements at Trapper Creek only include dust

210 particles smaller than 2.5 μm and are only compared with simulated dust concentrations at the

211 same size range. All other concentration measurements capture dust particles below 40 μm and

212 are compared with simulated dust over the whole size range ($< 10 \mu m$). The dust deposition

213 fluxes dataset, which including 84 stations, is also the same as Huneeus et al. (2011). The

214 locations of the observation network are shown in Figure 2d, with the AOD data taken close to

215   source regions and the dust surface concentrations and deposition fluxes measured at relatively

216   remote regions. The Pearson correlation coefficient (r) are provided for each comparison. We

217   note that the comparisons are subject to representative biases caused by comparing an

218   observational station with a global model grid point (with a horizontal resolution of ~ 100 km).

219   The comparisons of dust concentration and deposition flux also have systematic errors because

220   the measurements were for a different time period than that of the model simulation.

221   In general, the three comparisons indicate that our CTRL simulation is capable of capturing

222   the global dust cycle in both near the source and remote regions. As shown in Figure 2a, the

223   modeled AOD is within a factor of two of the observations over most of the stations. The

224   correlation of the AOD comparison is 0.73, which is comparable to the best performing

225   simulation (r = 0.72) in Kok et al. (2014b). Our model also does a fairly good job in simulating

226   the dust surface concentrations (Figure 2b) and produces a correlation coefficient of 0.84. For the

227   three high latitude sites, the model shows moderate underestimation at Heimaey and Trapper

228   Creek and large positive bias at Alert (see discussion below). The correlation coefficient for

229   simulated dust deposition fluxes (r = 0.48) is also within the range of the AeroCom comparisons

230   (0.08 to 0.84) in Huneeus et al. (2011). The model results over most of the sites are within one

231   order of magnitude difference, except at the polar regions. In particular, the model overestimates

232   the dust deposition flux in Greenland (red triangles in Figure 2c and 2d) by around two orders of

233   magnitude, likely due to too strong local emissions simulated near the coast of Greenland (Figure

234   1a).

235   The seasonal cycle of dust surface concentrations at the three Arctic stations (Heimaey, Alert,

236   and Trapper Creek) are shown in Figure 3, along with the contribution from seven tagged

237   sources. The simulated dust concentrations at Heimaey are dominated by HLD and agree well

238   with the observation in late summer and autumn (Figure 3a). Its annual-averaged low bias shown

239   in Figure 2b mainly comes from the springtime, when Prospero et al. (2012) found the observed

240   dust are related to dust storms in Iceland, indicating a possible underestimation in the simulated

241   Icelandic dust during this time. The HLD also dominates the surface dust concentrations at Alert

242   (Figure 3b), leading to a large overestimation from June to August in our simulation, which

243   possibly implies a high bias and wrong seasonal cycle of HLD emission over Greenland and

244   North Canada. The Trapper Creek station is instead dominated by LLD from East Asia and

245   shows an underestimation for most of the year. It is noted that we only include fine dust

246   (diameter < 2.5 μm) for the comparison at Trapper Creek. Larger size range is likely to be more

247   influenced by HLD sources. The low bias here, especially that during the autumn, can be related

248   to the missing of local emissions from the coast of Southern Alaska (Figure 1a) that occurs most

249   frequently in autumn (Crusius et al., 2011). An underestimation of the transport from Saharan

250   dust may also contribute slightly, as the influence from Saharan dust is found during mid-May at

251   Trapper Creek (Breider et al., 2014).

252   The simulated Arctic dust vertical profiles are also compared with the measured dust

253   concentrations during the Arctic Research of the Composition of the Troposphere from Aircraft

254   and Satellites (ARCTAS) flight campaign (Figure 4) (Jacob et al., 2010). The ARCTAS

255   campaign was conducted over the North American Arctic in April and July 2008. The simulated

256   profiles are averaged over the regions where the aircraft flew, in accordance with Groot

257   Zwaaftink et al. (2016). In April, the model does a good job in capturing the Arctic dust vertical

258   profiles (Figure 4a). However, in July, the model underestimates dust by a factor of 2 to 5

259   between 3 and 10 km (Figure 4b). It also shows an overestimation near the surface in July, which

260   agrees with the surface concentrations comparison at Alert station (Figure 3b). The

261   underestimation in the upper troposphere and overestimation near the surface likely imply a too

262   weak vertical transport of HLD in the North American Arctic in summertime. The high bias in

263   the upper troposphere may also be related to an underrepresentation of LLD transport.

264   Finally, we evaluate the simulated dust extinction against the Cloud-Aerosol Lidar and

265   Infrared Pathfinder Satellite Observation (CALIPSO) retrieval (Luo et al., 2015a, b; Yang et al.,

266   2022), which includes nighttime dust extinction for the period of 2007 to 2009. This data set has

267   improvements in dust separation from other aerosol types and thin dust layer detection in the

268   Arctic compared to the standard Cloud-Aerosol Lidar with Orthogonal Polarization (CALIOP)

269   Level 2 product (Winker et al., 2013). To make an apple-to-apple comparison, the modeled dust

270   extinction is sampled along the CALIPSO tracks and screened by cloud fraction (Wu et al.,

271   2020). For this comparison, we only use the first three years (2007 to 2009) of the CTRL

272   simulation to be consistent with the observation period. Overall, the model does a good job in

273   capturing the Arctic dust extinction vertical profiles (Figure 5). We notice that the simulated dust

274   extinction is lower than CALIPSO retrievals at the upper troposphere in summer, which agrees

275   with the ARCTAS comparisons. The simulated dust extinction also shows a consistent

276   underestimation in springtime (MAM) and a near surface underestimation in wintertime (MAM).

277   Since the Arctic is mostly covered by ice and snow in these two seasons, the impacts of HLD are

278   expected to be limited and the low biases are most likely due to the underprediction of LLD

279   transport. The near surface underestimation in DJF may indicate a too weak LLD transport in the

280   lower troposphere (e.g., the transport of dust emitted from Central Asia; see Figure 7 and the

281   corresponding discussions in Section 3.2). Moreover, the HLD has a large contribution in the

282   lower troposphere in boreal summer and autumn, which is consistent with its strong emission at

283   that time. In contrast, LLD plays a more dominant role in the upper troposphere, where African

284   dust contributes the most in the springtime and East Asian dust has a larger contribution in the

285   other seasons.

286   **3.2 Arctic dust mass source attribution**

287   Table 2 summarizes the relative contributions from individual sources to the total Arctic dust

288   burden. The transport pathways can be identified from the dust burden spatial distribution for

289   each source in Figure 6, while the relative contribution of each source to the total dust burden is

290   shown in Figure S2. We also calculate the regional burden efficiency for each source (Table S1),

291   which is defined as the mean contribution to the Arctic dust column burden divided by the

292   corresponding dust emission (H. Wang et al., 2014). This metric represents the sensitivity of

293   Arctic dust loading to per unit change of dust emission from each source (i.e., the poleward

294   transport efficiency of each source).

295   Our model results suggest that the HLD (Arc) is the largest contributor (30.7%) to the annual

296   mean Arctic dust burden among all the tagged sources. As shown in Figure 6a and Figure S2a,

297   the local dust is confined within the high latitudes, with the higher amounts and higher

298   contributions to the total dust burden near the sources in North Canada, coast of Greenland, and

299   Iceland. The interior of the Greenland ice sheet, with its higher elevations, is more influenced by

300   LLD from North Africa and East Asia than HLD (Figure S2c and S2f). This is due to the weak

301   vertical transport of local emissions in the Arctic (see more discussions below).

302   On the other hand, all LLD sources are responsible for 69.3% of the dust loading in the Arctic,

303   with considerable contributions from North Africa (24.2%) and Asia (in total 44.2%; EAs:

304   19.9%, MSA: 11.5%, CAs: 12.8%), and minor contributions from NAm (0.1%) and RoW (nearly

305   0). The North African dust is primarily transported westward to the Atlantic and southward to

306   Sahel, with a smaller fraction transported directly northward or northeastward across the Eurasia

307 to the Arctic (Figure 6c; Shao et al., 2011). The westward trajectory can also bring dust to the

308 Arctic through the Azores high (e.g., VauCuren et al., 2012), but this pathway is not clearly seen

309 on Figure 6c likely due to the strong wet removal process over the North Atlantic. As evident by

310 the low transport efficiency in Table S1, the significant contribution of the North African dust to

311 the Arctic dust burden is mainly due to its massive emission. However, this is not the case for

312 EAs. The East Asian dust is first lifted vertically by topography and convection (Shao et al.,

313 2011) and is widely spread over the Northern Hemisphere mid- and high-latitude regions through

314 the westerly flow in the upper troposphere (Figure 6f). The high elevation of East Asian dust

315 plumes results in weaker removal processes and thus an efficient poleward transport. As shown

316 in Table S1, the annual transport efficiency of the East Asian dust is relatively high among the

317 LLD sources, which is nearly three times larger than that of the North African dust. The

318 poleward transport of dust from CAs and MSA both takes the pathway across Siberia (Figure 6d

319 and 6e). The transport efficiency of the CAs dust is two times higher than that of the MSA dust

320 (Table S1). This is attributed to CAs being closer to the Arctic and having less southward dust

321 transport than MSA. Overall, the LLD from North Africa and Asia contributes more to the

322 Eurasia and Pacific sector of the Arctic (Figures S2c to S2f). The impact of NAm dust is limited

323 by its weak emission (Figure 6b), while dust emitted in the Southern Hemisphere (RoW) can

324 hardly pass the equator (Figure 6g).

325 Earlier modeling studies (Breider et al., 2014; Groot Zwaaftink et al., 2016; Luo et al., 2003;

326 Tanaka and Chiba, 2006) also quantify the relative contributions of dust from various regions to

327 the Arctic dust loading. Among these studies, only Groot Zwaaftink et al. (2016) includes HLD.

328 Our estimate about the HLD percent contribution is close to that from their study (27%). For

329 LLD, our conclusion about the dominant role of African and Asian dust to the Arctic dust burden

330 is also corroborated by these previous studies. However, the relative importance of African and

331 Asian dust is uncertain. Based on our results, the Asian dust is responsible for 65% of the LLD

332 transport to the Arctic, while the African dust only contributes 35%. Other studies find that 50%

333 (Groot Zwaaftink et al., 2016; Luo et al., 2003; Tanaka and Chiba, 2006) to as much as 65%

334 (Breider et al., 2014) of the LLD in the Arctic is attributed to North Africa. These discrepancies

335 may be explained by the different dust emission and scavenging, dust size distribution,

336 meteorological fields, and/or time periods for the model simulation. For example, the wet

337 removal process is expected to have large discrepancies among different models, because of the

338 large uncertainties in the model representation of clouds and precipitation. The different spatial

339 distributions of dust emission due to the use of different emission parameterizations may also

340 contribute to the discrepancies (e.g., North Africa dust in our study contributes slightly less

341 (51.9%) to the global dust emission than the other studies (from 57% to 67%). Isotopic analysis

342 (Bory et al., 2002, 2003) and case studies (Huang et al., 2015; Stone et al., 2005; VanCuren et al.,

343 2012) have proved that both Asian and African dust can be transported to the Arctic. However, it

344 remains unclear which of them contributes more to the Arctic dust loading due to the limited

345 observational constraints.

346 HLD and LLD source regions also have very distinct vertical distributions in the Arctic.

347 Figures 7a and 7b show the annual mean vertical profiles of Arctic dust concentrations from

348 various sources and their percentage contributions, respectively. The Arctic dust in the lower

349 atmosphere is dominated by the local source. HLD accounts for more than 30% of the Arctic

350 dust concentrations below 800 hPa, with up to 85% contribution near the surface. However, the

351 HLD contribution decreases rapidly with height and is less than 10% above 700 hPa. This is

352 because the lower troposphere of the Arctic is more stratified than the mid- and low latitudes,

353 which suppresses the vertical transport of HLD. The lower tropospheric stability (LTS) from the

354 CTRL simulation and comparison with the MERRA2 reanalysis data are shown in Figure S3.

355 The weak HLD vertical transport in the Arctic is also reported by previous studies (Groot

356 Zwaaftink et al., 2016, Baddock et al., 2017; Bullard, 2017). Moreover, the LTS over the Arctic

357 sea ice is much larger than that over open ocean surface (Schweiger et al., 2008), which may lead

358 to a stronger vertical transport of HLD over open waters. This suggests that the vertical transport

359 of HLD may change with the sea ice reduction in a warming future.

360   In contrast, LLD has a higher contribution in the mid- and upper troposphere than near the

361 surface. Such a vertical distribution of LLD is consistent with Stohl (2006) and Groot Zwaaftink

362 et al. (2016). As Stohl (2006) found, aerosols originating from the warm subtropics are

363 transported poleward following the uplifted isentropes and the Arctic lower atmosphere is

364 dominated by the near-impenetrable cold polar dome. Therefore, there is a slantwise lifting of

365 low latitude aerosols during their poleward transport. NAf and EAs are the two key contributors

366 to the Arctic dust vertical concentrations, each of which contributes up to one third of the total

367 dust concentrations above 700 hPa. Dust emission from MSA also has a moderate contribution

368 (15-20%) that increases gradually with height, while the contribution from CAs peaks at 700 to

369 800 hPa, indicating a lower altitude transport pathway than the EAs and MSA dust.

370   In addition, the Arctic dust undergoes a strong seasonal cycle (Table 2 and Figures 7c-j).

371 Because of the strong local emissions (Figure 1c), about half of the Arctic dust burden in

372 summer and autumn come from HLD, with more than 50% contribution of Arctic dust

373 concentrations below 850 hPa in these two seasons. In contrast, LLD plays a dominant role in

374 spring and winter. The North African dust has the largest contribution in spring, which accounts

375 for about 45% of the total dust concentrations above 700 hPa. The East Asian dust is more

376   important in the other three seasons. Due to its high emission height, the relative contribution

377   from EAs tends to increase with height and reaches 30% to 50% of the total dust concentration

378   above 500 hPa in summer, spring, and winter.

379   **3.3 Immersion freezing on dust in the AMPCs**

380   We are particularly interested in the contribution of various dust sources to the Arctic INP

381   populations. Therefore, we compare the simulated INP concentrations with nine Arctic field

382   measurements, which are summarized in Table 3. The modeled dust INP concentrations are

383   diagnosed from monthly averaged aerosol properties using the default CNT scheme and two

384   empirical ice nucleation parameterizations, DeMott et al. (2015; hereafter as D15) and Sanchez-

385   Marroquin et al. (2020; hereafter as SM20). The D15 parameterization, which is representative

386   of Saharan and Asian desert dust, relates dust INP number concentrations to the number

387   concentration of dust particles larger than 0.5 μm diameter and is found to produce the most

388   reasonable LLD INP concentrations in EAMv1 (Shi and Liu, 2019). CNT and D15 are applied to

389   LLD only and all the dust aerosols (LLD and HLD) in Figures 8a-b and Figures 8d-e,

390   respectively. The SM20 parameterization, which is derived for the HLD Icelandic dust, describes

391   the dust INP number concentrations as a function of surface active site density and total dust

392   surface area. Considering the possibly different ice nucleation ability between HLD and LLD,

393   we only applied the SM20 parameterization to HLD and the CNT and D15 parameterizations are

394   still applied to LLD in Figures 8c and 8f, respectively. To account for the contributions from

395   other aerosol types, we also calculate the INP concentrations from BC (Fig. 8g) and sea spray

396   aerosol (SSA; includes MOA and sea salt) (Fig. 8h) following Schill et al. (2020; hereafter as

397   Sc20) and McCluskey et al. (2018; hereafter as M18), respectively. More details about the ice

398   nucleation parameterizations are provided in Text S2. We discuss the choice of dust ice

399   nucleation schemes in Text S2.6 in the Supplement.

400   Overall, only including LLD as INPs results in up to four orders of magnitude underprediction

401   compared to observations (Figures 8a and 8d), while taking into account the contribution from

402   HLD greatly improves the model performance by increasing the simulated dust INP

403   concentrations (Figures 8b, 8c, 8e, and 8f). The CNT parameterization produces 5 to 10 times

404   more INP concentrations than the other two schemes at moderately cold temperatures (-22 to -

405   28℃), while it has a significant underestimation of observed INP concentrations at warm

406   temperatures (T > -18℃) (also see Figure S4). D15 and SM20 agree well with each other in

407   simulating HLD INPs, with SM20 producing slightly higher results than D15. Our modeling

408   results also indicate that BC and SSA have much less contributions to INP than dust in all the

409   nine field campaigns (Figure 8g and 8h).

410   A detailed analysis of sources of the INPs for the nine datasets based on modeling analyses

411   and the corresponding observations in the literature are provided in Table 3. Modeling results

412   indicate that HLD has larger contributions to the INPs for the campaigns conducted in summer

413   and autumn than spring, in agreement with the observations. Also, ground-based measurements

414   are more influenced by the nearby HLD sources, while LLD from EAs and NAf contributes

415   more to the aircraft measurements.

416   Our modeling analyses about the INP sources agree well with the observational studies at

417   Alert in spring 2016 and near Iceland in autumn 2014 (symbol "C" and "I" in Figure 8,

418   respectively), while the model underestimates the observed INP concentrations in both cases.

419   The low bias in dataset C indicates an underprediction in the long-range transport of Asian dust

420   to the Arctic surface in springtime. The underestimation in dataset I is more likely due to the fact

421   that some of the aircraft measurements were taken inside the Icelandic dust plumes (Sanchez-

422   Marroquin et al., 2020), which cannot be resolved by the monthly mean model output and the

423   coarse model horizontal resolution (1°). Such uncertainties exist in all the model-observation

424   comparisons.

425   Some other comparisons in INP sources reveal the lack of marine and carbonaceous INPs in

426   the model. The model results show a dominance of dust INPs in spring 2017 at Zeppelin and

427   Oliktok Point (symbol "D" and "E" in Figure 8) and in Autumn 2004 at Utqiaġvik (symbol "H"

428   in Figure 8), while the observational studies suggested the importance of marine sources at the

429   first two locations and of carbonaceous aerosols at Utqiaġvik. Therefore, it is likely that the

430   model underestimates the contribution of MOA (Wilson et al., 2015; Zhao et al., 2021a) and

431   does not account for terrestrial biogenic INPs (Creamean et al., 2020) due to the lack of

432   treatments in the model. In addition, both D15 and SM20 schemes cannot represent the high ice

433   nucleating ability of HLD at warm temperatures at Zeppelin in summer 2016 (symbol "G" in

434   Figure 8), which is attributed to soil organic matter by Tobo et al. (2019). When these organics

435   are taken into account in the model, model overestimation for site G will get even worse,

436   implying an overestimation of surface dust concentrations and/or HLD dust emission at Svalbard

437   in the summertime. In summary, the model's INP biases in the Arctic are likely due to biases in

438   the simulated aerosol fields (e.g., dust, MOA, and BC) and uncertainties in current ice nucleation

439   parameterizations or missing representations of other INP sources (e.g., terrestrial biogenic

440   aerosols).

441   In addition, we do not explicitly represent the potential ice nucleation ability differences in

442   freshly emitted HLD and long-range transported LLD caused by the aging and the coatings of

443   pollutants (Kulkarni et al., 2014; Boose et al., 2016). However, D15 and SM20 may already take

444   the aging effect into account implicitly. Because D15 is based on the Saharan and Asian dust

445   data collected over the Pacific Ocean basin and US Virgin Islands, respectively, which are far

446   away from the corresponding LLD sources, while SM20 is derived from the freshly emitted

447   Icelandic HLD, which is subjected to less aging effect.

448   The comparisons above are based on INP concentrations at a given temperature set by the INP

449   instruments, which reflects the potential INP populations under ambient aerosol conditions. Next,

450   we examine the immersion freezing rate of dust originating from the seven tagged sources

451   (Figure 9) to evaluate the influences of HLD and LLD on ice nucleation processes in mixed-

452   phase clouds. It is noted that the immersion freezing rate here is calculated online in the model

453   using the ambient temperature and the default CNT ice nucleation parameterization.

454   Compared with its contribution to the dust burdens, the contribution of the HLD to the annual

455   mean mixed-phase cloud immersion freezing rate is relatively small (~10% below 600 hPa)

456   (Figure 9a). This is because the HLD is mainly located in the lower troposphere and not a lot of

457   HLD can reach the mixed-phase cloud levels (or the freezing level), especially under the case

458   that the HLD tends to be more prevalent in the warm seasons (see more discussion below).

459   Among the LLD sources, North African dust (Figure 9c) and East Asian dust (Figure 9f) are the

460   two major contributors, both of which are responsible for more than 20% of the annual mean

461   immersion freezing rate in the mixed-phase clouds. Consistent with the vertical distribution of

462   dust concentrations, the North African dust has its maximum contribution (30-40%) at around

463   500 hPa, while the East Asian dust plays a more important role at higher altitudes (above 400

464   hPa). Dust from Central Asia also has a moderate contribution (~20%) to the immersion freezing

465   rate in the Arctic (Figure 9d).

466   Considering the different seasonality of HLD and LLD in the Arctic, we next investigate the

467   seasonal variations of the immersion freezing rate in the Arctic mixed-phase clouds from HLD

468   and two dominating LLD sources (NAf and EAs) (Figure 10). HLD has the largest contribution

469   to the Arctic immersion freezing rate in boreal autumn, with more than 30% below 700 hPa and

470   up to 50% near the surface (Figure 10c). It is related to the prevalence of HLD and relatively

471   cold temperatures during this time in the Arctic. This is not the case for the summer, when the

472   freezing level is relatively high. Although it is responsible for 50% of the total Arctic dust

473   burden in the boreal summer, HLD has a limited contribution to the immersion freezing rate in

474   the clouds (Figure 10b), because its weak vertical transport makes it hard to reach the freezing

475   line. The contrast results in summer and autumn suggest that the immersion freezing rate in the

476   Arctic clouds is influenced by air temperature in addition to the aerosols. It also implies that the

477   surface INP measurements may not reflect the complete picture of INP effects and more aircraft

478   INP measurements are needed in the future. The seasonal variations of the immersion freezing

479   rate from NAf and EAs are weaker than that from HLD but are still subjected to the vertical

480   temperature change with season. The North African dust contributes more in spring and winter,

481   while the East Asian dust is more important in summer and autumn.

482   **3.4 Impact on cloud properties and radiative fluxes**

483   Dust INPs can freeze the supercooled liquid droplets, which impacts the cloud microphysical

484   and macrophysical properties and modulates the Earth's radiative balance. To examine such

485   impacts, we conduct three sensitivity experiments that turn off the heterogeneous ice nucleation

486   in the mixed-phase clouds by dust from Arctic local source, North Africa, and East Asia,

487   respectively (i.e., noArc, noNAf, and noEAs in Table 1). The impacts of dust INPs from each

488   source are determined by subtracting the respective sensitivity experiment from CTRL. Due to

489 the feedbacks in dust emission and wet scavenging caused by changing cloud properties, the dust

490 concentrations in the sensitivity experiments are not identical to CTRL, but the absolute

491 differences are mostly within 5% (Figure S5 in the Supplement).

492 The cloud liquid and ice changes caused by dust INPs from each source are shown in Figure

493 11. Due to the strengthening of heterogeneous ice nucleation processes, INPs from all the three

494 sources consistently reduce the total liquid mass mixing ratio (TLIQ) (Figure 11, first column)

495 and cloud liquid droplet number concentration (NUMLIQ) (Figure 11, third column). The

496 influence of HLD is mainly in the lower troposphere (Fig. 11, top row) and the influence of LLD

497 extends to higher altitudes (Fig. 11, bottom two rows). Moreover, the cloud ice number

498 concentration (NUMICE) decreases in the upper troposphere (Figure 11, fourth column), likely

499 due to less cloud droplets available for the homogeneous freezing in cirrus cloud after

500 introducing dust INPs in the mixed-phase clouds. With fewer ice crystals falling from the cirrus

501 clouds to the mixed-phase clouds, the WBF process in the mixed-phase clouds is inhibited

502 (Figure S6). Other ice phase processes such as the accretion of cloud water by snow and the

503 growth of ice crystals by vapor deposition also become less efficient, which decreases the total

504 ice mass mixing ratio (TICE) above 600-700 hPa altitude (Figure 11, second column). TICE in

505 the lower troposphere is increased because of immersion freezing and snow sedimentation from

506 above.

507 Since liquid water path (LWP) is found to play a critical role in the Arctic radiative budget

508 (e.g., Dong et al., 2010; Hofer et al., 2019; Shupe and Intrieri, 2004), we further investigate the

509 seasonal variations of LWP changes caused by dust INPs from the three sources (Figure 12).

510 Corroborated with their large contribution to the immersion freezing rate during this time (Figure

511 10, top row), HLD INPs produce the strongest LWP decrease (-1.3 g m^{-2}) in boreal autumn

512 (Figure 12c), especially over North Canada and Greenland. The influence of LLD INPs on LWP

513 peaks in spring and winter. North African dust tends to have a larger impact on North Eurasia,

514 while East Asian dust impacts the west Arctic more.

515   Dust INPs from the three sources consistently increase (decrease) the annual mean

516 downwelling shortwave (longwave) radiative flux (FSDS and FLDS) at the surface (Figure 13,

517 left and middle columns). This is mainly due to the LWP decrease, which reduces the cloud

518 albedo and longwave cloud emissivity. For HLD INPs, the FLDS reduction dominates over the

519 FSDS increase and causes a net cooling effect at the Arctic surface (-0.24 W m^{-2}) (Figure 13c).

520 In contrast, FSDS and FLDS changes related to the LLD INPs are comparable, which cancels

521 each other and yields a small net radiative effect (0.08 W m^{-2} for NAf and -0.06 W m^{-2} for EAs)

522 (Figure 13, bottom two rows). These differences in the net radiative effect are associated with

523 different seasonalities of HLD and LLD. The insolation in the Arctic is strong in spring and

524 summer but very limited in autumn and winter. Since the HLD INPs have much stronger

525 influence on LWP in autumn and winter than spring and summer (Figure 12), their contribution

526 to the FSDS warming is weak and the FLDS cooling in autumn and winter dominates the annual

527 mean effect (Table 4, part 1; also seen in Figure S7 to S9). LLD INPs are also important in

528 spring and summer, so their FSDS warming effect is comparable to, and compensates for, the

529 FLDS cooling effect.

530   We also examined the dust INP effect on cloud radiative forcing (CRF) at the top of the

531 atmosphere (TOA) (Table 4, part 2). Dust INPs from the three sources induce a small net cooling

532 (from -0.03 to -0.05 W m^{-2}) in the Arctic, with SW warming and LW cooling effects. The net

533 cooling persists throughout the year, except for the summertime when the sufficient insolation

534 results in a strong SW warming and, consequently, a net warming effect. Shi and Liu (2019) also

535   found LLD can induce a generally net cooling effect above 70°N (0.18 to -1.95 W m^{-2}), but in a

536   much higher magnitude than the sum of NAf and EAs dust INP effects (-0.15 W m^{-2} above 70°N,

537   not shown in Table 4), which implies the aerosol glaciation effect on mixed-phase clouds is

538   highly non-linear.

539   Finally, we evaluate the model performance in simulating the Arctic LWP and radiative fluxes

540   against the Moderate Resolution Imaging Spectroradiometer (MODIS) LWP and the Cloud and

541   the Earth's Radiant Energy System Energy Balanced and Filled Edition 4.1 (CERES-EBAF

542   Ed4.1) products (Loeb et al., 2018; Kato et al., 2018), respectively (Figure 14). Two MODIS

543   datasets are used, including the standard Collection 6.1 product (Pincus et al., 2012; P12) and

544   Khanal et al. (2020; K20). The P12 product combines MODIS observations from Terra and Aqua

545   and is designed for apples-to-apples comparisons with modelling results from the Cloud

546   Feedback Model Intercomparison Project (CFMIP) Observation Simulator Package (COSP). The

547   standard product has a well-known positive zonal bias near the poles that is strongly correlated

548   with the solar zenith angle (SZA). The K20 product largely reduces this bias by utilizing the

549   SZA and cloud heterogeneity index in their retrieval algorithm. The MODIS simulator is used

550   for to calculate the simulated LWP. According to Fig. 14, the simulated LWP from the four

551   experiments are lower than P12 but higher than K20. All the four experiments also underestimate

552   FSDS with too strong SWCF and overestimate FLDS with too strong LWCF, which likely points

553   to the biases of modeled clouds (e.g., too much LWP as compared to K20). The differences

554   among the model experiments are very small compared to their discrepancies with observations.

555   We notice including dust INPs from the three sources decreases the simulated LWP (i.e., CTRL

556   has less LWP than the other experiments) (Figure 14a), which makes the model performance

557   better if compared to K20. Moreover, it shows noticeable improvements in simulating both

558 surface and TOA radiative fluxes after including dust INPs from each of the three sources (i.e.,

559 the results from CTRL are closer to the CERES results than the other three experiments) (Figure

560 14b-e).

561   Overall, including HLD or LLD INPs do not contribute a lot to the reduction of biases in

562 simulating the LWP and radiative fluxes in the AMPCs. However, the representation of AMPCs

563 in global climate models is associated with multiple cloud macro- and microphysical processes,

564 and large-scale dynamics (Morrison et al., 2012) (see more discussion in Section 4), which

565 interact with one another non-linearly. Therefore, even though including HLD or LLD INPs do

566 not improve the representation of AMPCs significantly in our model, a good representation of

567 dust INPs, especially including HLD INPs, could still be of great importance for parameterizing

568 AMPCs in the model.

569 **4. Discussion**

570   The HLD emission in our CTRL simulation is manually tuned up by 10 times to match the

571 estimate by Bullard et al. (2016), which is derived by compiling field measurements in Iceland

572 and Alaska. Since the instruments were operated under extreme Arctic conditions and the

573 sampling is very scarce, this estimate may have large uncertainties. Therefore, the tuned HLD

574 emission can be biased as well. Considering the overestimation of Greenland dust deposition,

575 summertime surface dust concentrations at Alert station, and surface INP concentrations at

576 Svalbald, our tuning may cause a regional and temporal high bias in HLD dust emissions. We

577 examine this uncertainty by conducting a sensitivity experiment with halving HLD emissions in

578 CTRL (i.e., HLD_half) and analysing the interannual variability of CTRL and HLD_half

579 simulations (Table S2 and Figures S10-S11). The HLD_half simulation indeed has a better

580 performance than CTRL. However, the high bias for Greenland deposition and the summertime

581 overestimation of Alert dust surface concentration still exist, which reflects the limitation of the

582 dust emission parameterization we use. This parameterization may not be able to capture the

583 spatial distribution of dust emissions across the Arctic, considering that the model performance

584 at other sites is much better (e.g., Heimaey, Figure 3a). Also, the HLD emissions and their

585 regional distributions have large interannual variabilities. Therefore, as we mentioned in Section

586 3.1, comparing model simulations with measurements conducted in different years may result in

587 large uncertainties.

588 The overestimation of surface dust and INP concentrations may imply a too weak vertical

589 transport of HLD, considering the low biases of dust in the upper troposphere as compared with

590 ARCTAS measurements and CALIPSO retrievals. The weak vertical transport at the source

591 regions in EAMv1 was also found in Wu et al. (2020), which was related to the too strong dry

592 deposition at the surface layer. If this bias is addressed, HLD would contribute less (more) to the

593 Arctic dust concentrations in the lower (upper) troposphere, which suggests a larger contribution

594 of HLD to the heterogeneous ice nucleation in the mixed-phase clouds in the summertime. As a

595 result, the HLD would induce a more positive net downwelling radiative flux at the surface in

596 summer and a less negative annual mean radiative effect. It is also noted that the underprediction

597 in the upper troposphere dust may come from a weak long-range transport of LLD. If this is the

598 case, the HLD would have a weaker contribution to the upper level dust concentrations and

599 likely less of an impact on mixed-phase cloud heterogeneous ice nucleation in the summertime.

600 In addition, EAMv1 has intrinsic biases in its cloud microphysics parameterizations. As

601 mentioned in Section 2.1, the WBF process rate in EAMv1 is tuned down by a factor of 10,

602 which results in too many supercooled liquid clouds in high latitudes (Y. Zhang et al., 2019; M.

603   Zhang et al., 2020). Shi and Liu (2019) found the sign and magnitude of dust INP cloud radiative

604   effect in the Arctic would change, after removing the tuning factor for the WBF process in

605   EAMv1. Moreover, EAMv1 does not account for several secondary ice production mechanisms,

606   which are suggested to have a large impact on the ice crystal number concentrations and thus

607   cloud phase (Zhao and Liu, 2021; Zhao et al., 2021b). All these uncertainties in the cloud

608   microphysical processes would interact non-linearly and influence our estimate of INP radiative

609   effect and should be addressed in future studies.

610   **5. Conclusions**

611   In this study, we investigate the source attribution of dust aerosols in the Arctic and quantify

612   the relative importance of Arctic local dust versus long-range transported LLD to the Arctic dust

613   loading and INP population. We found that HLD is responsible for 30.7% of the total dust

614   burden in the Arctic, whereas LLD from Asia and North Africa contributes 44.2% and 24.2%,

615   respectively. The vertical transport of HLD is limited due to the stable cold air in the Arctic and

616   thus it contributes more to the dust burden in the lower troposphere. In boreal summer and

617   autumn when the contribution of HLD is at a maximum because of stronger local dust emissions,

618   HLD is responsible for more than 30% of the Arctic dust loading below 800 hPa, but less than 10%

619   above 700 hPa. In contrast, LLD from North African and East Asian dust dominates the dust

620   burden in the free troposphere, since the poleward transport of LLD follows the uplifted

621   isentropes. The North African and East Asian dust accounts for about two thirds of the dust

622   loading above 700 hPa, with the remaining one third from other LLD sources. The North African

623   dust contributes more between 500 and 700 hPa, while the East Asian dust dominates in the

624   upper troposphere (above 400 hPa) because of its high emission heights. In addition, the North

625 Africa source has a larger contribution in springtime, while the other three seasons are more

626 influenced by the East Asian source.

627 Modeled dust INP concentrations are investigated following three ice nucleation

628 parameterizations: CNT, D15 and SM20. Compared with INP measurements, our results show

629 that including HLD as INPs significantly improves the model performance in simulating Arctic

630 INP concentrations, especially for the ground measurements and for the measurements

631 conducted in summer and autumn. We also examine the INP contributions from BC and SSA

632 based on Sc20 and M18, respectively. The model suggests that both of them are only weak

633 sources compared with dust. We note that the model may underestimate SSA INPs and currently

634 misses the representation of terrestrial biological INPs. The model biases of INPs can also be due

635 to bias in simulating Arctic dust concentrations and/or the uncertainties in ice nucleation

636 parameterizations.

637 We examine the contribution of dust from the three sources (Arctic, North Africa, and East

638 Asia) to the ambient immersion freezing rate in the Arctic. The contribution from HLD shows a

639 strong seasonal variation, with the peak contribution in boreal autumn (above 20% below 500

640 hPa). In summer, although HLD has strong contributions to the dust loading and INP

641 concentrations in the lower troposphere, its impact on the ambient immersion freezing rate is

642 limited due to the warm temperatures and weak vertical transport. This finding implies that

643 surface INP measurements may not be sufficient in representing the INP population in the Arctic

644 mixed-phase clouds and more measurements of INP vertical profiles are needed in the future.

645 North African and East Asian dust are the two major LLD contributors to the ambient immersion

646 freezing rate. The annual mean contribution (30-40%) from North African dust peaks at around

647   500 hPa, while the immersion freezing is dominated by East Asian dust (more than 40%) in the

648   upper troposphere (above 400 hPa).

649   The cloud glaciation effects of dust INPs from local Arctic sources, and North African and

650   East Asian sources, are further examined. It is found that INPs from all the three sources

651   consistently result in a reduction in TLIQ and NUMLIQ. TICE and NUMICE at higher altitude

652   also decrease, likely due to the weakening of homogeneous freezing in cirrus clouds. LWP

653   reduction caused by HLD INPs is evident in autumn and winter, while those by dust INPs from

654   the two LLD sources peak in spring. HLD INPs also drive a net cooling effect of -0.24 W m^{-2} in

655   the downwelling radiative flux at the surface in the Arctic, while the net radiative effects of the

656   two LLD INP sources are relatively small (0.08 W m^{-2} for NAf and -0.06 W m^{-2} for EAs). This

657   variation in radiative effect reflects the seasonal difference between HLD and LLD. Our results

658   also suggest that all the three dust sources result in a weak negative net cloud radiative effect (-

659   0.03 to -0.05 W m^{-2}) in the Arctic, which is consistent with Shi and Liu (2019).

660   Overall, our study shows that the Arctic local dust, which has been overlooked in previous

661   studies, may have large contributions to the Arctic dust loading and INP population. It can also

662   influence the Arctic mixed-phase cloud properties by acting as INPs. Considering the climate

663   impacts of local Arctic dust emissions will be important given a warming climate, where

664   reduction in snow coverage and more exposure of dryland in the Arctic may lead to increased

665   HLD emissions.

666 *Code availability.* The E3SM code is available on GitHub: https://github.com/E3SM-
667 Project/E3SM.git.

668 *Author contribution.* YS and XL conceived the project. YS modified the code, conducted the
669 simulations, and led the analyses with suggestions from XL, MW, XZ, ZK, and HB. XL
670 supervised the study. YS wrote the first draft of the paper. All coauthors were involved in helpful
671 discussions and revised the paper.

672 *Competing interests.* The authors declare that they have no conflict of interest.

673 *Acknowledgements.* The authors would like to thank Kang Yang and Dr. Zhien Wang for
674 providing the CALIPSO dust extinction retrievals and Drs. Meng Zhang and Sarah Brooks for
675 their comments and suggestions. Mingxuan Wu is supported by the US Department of Energy
676 (DOE), Office of Biological and Environmental Researsch, Earth and Environmental System
677 Modeling program as part of the Energy Exascale Earth System Model (E3SM) project. The
678 Pacific Northwest National Laboratory (PNNL) is operated for DOE by the Battelle Memorial
679 Institute under contract DE-AC05-76RLO1830. This research used resources of the National
680 Energy Research Scientific Computing Center, a DOE Office of Science User Facility supported
681 by the Office of Science of the U.S. Department of Energy under contract DE-AC02-
682 05CH11231.

683 *Financial support.* This research was supported by the DOE Atmospheric System Research
684 (ASR) Program (grants DE-SC0020510 and DE-SC0021211).

References

Albani, S., Mahowald, N. M., Perry, A. T., Scanza, R. A., Zender, C. S., Heavens, N. G., Maggi, V., Kok, J. F., and Otto-Bliesner, B. L.: Improved dust representation in the Community Atmosphere Model, J. Adv. Model. Earth Syst., 6, 541–570, https://doi.org/10.1002/2013MS000279, 2014.

Arimoto, R., Duce, R. A., Ray, B. J., Ellis Jr, W. G., Cullen, J. D., and Merrill, J. T.: Trace elements in the atmosphere over the North Atlantic, J. Geophys. Res. Atmos., 100(D1), 1199–1213, https://doi.org/10.1029/94JD02618, 1995.

Arnalds, O., Dagsson-Waldhauserova, P., and Olafsson, H.: The Icelandic volcanic aeolian environment: Processes and impacts — A review, Aeolian Res., 20, 176–195, https://doi.org/10.1016/j.aeolia.2016.01.004, 2016.

Atkinson, J. D., Murray, B. J., Woodhouse, M. T., Whale, T. F., Baustian, K. J., Carslaw, K. S., Dobbie, S., O'Sullivan, D., and Malkin, T. L.: The importance of feldspar for ice nucleation by mineral dust in mixed-phase clouds, Nature, 498, 355–358, https://doi.org/10.1038/nature12278, 2013.

Baddock, M. C., Mockford, T., Bullard, J. E., and Thorsteinsson, T.: Pathways of high-latitude dust in the North Atlantic, Earth Planet. Sci. Lett., 459, 170–182, https://doi.org/10.1016/j.epsl.2016.11.034, 2017.

de Boer, G., Morrison, H., Shupe, M. D., and Hildner, R.: Evidence of liquid dependent ice nucleation in high-latitude stratiform clouds from surface remote sensors, Geophys. Res. Lett., 38, L01803, https://doi.org/10.1029/2010GL046016, 2011.

Bogenschutz, P. A., Gettelman, A., Morrison, H., Larson, V. E., Craig, C., and Schanen, D. P.: Higher-order turbulence closure and its impact on climate simulations in the community atmosphere model, J. Clim., 26, 9655–9676, https://doi.org/10.1175/JCLI-D-13-00075.1, 2013.

Boose, Y., Sierau, B., García, M. I., Rodríguez, S., Alastuey, A., Linke, C., Schnaiter, M., Kupiszewski, P., Kanji, Z. A., and Lohmann, U.: Ice nucleating particles in the Saharan Air Layer, Atmos. Chem. Phys., 16, 9067–9087, https://doi.org/10.5194/acp-16-9067-2016, 2016.

Bory, A. J.-M., Biscaye, P. E., Svensson, A., and Grousset, F. E.: Seasonal variability in the origin of recent atmospheric mineral dust at NorthGRIP, Greenland, Earth Planet. Sci. Lett., 196, 123–134, https://doi.org/10.1016/S0012-821X(01)00609-4, 2002.

Bory, A. J.-M., Biscaye, P. E., and Grousset, F. E.: Two distinct seasonal Asian source regions for mineral dust deposited in Greenland (NorthGRIP), Geophys. Res. Lett., 30, https://doi.org/10.1029/2002GL016446, 2003.

Breider, T. J., Mickley, L. J., Jacob, D. J., Wang, Q., Fisher, J. A., Chang, R. Y.-W., and Alexander, B.: Annual distributions and sources of Arctic aerosol components, aerosol optical depth, and aerosol absorption, J. Geophys. Res. Atmos., 119, 4107–4124, https://doi.org/10.1002/2013JD020996, 2014.

722   Bullard, J. E.: The distribution and biogeochemical importance of high-latitude dust in the Arctic
723   and Southern Ocean-Antarctic regions, J. Geophys. Res. Atmos., 122, 3098–3103,
724   https://doi.org/10.1002/2016JD026363, 2017.

725   Bullard, J. E. and Austin, M. J.: Dust generation on a proglacial floodplain, West Greenland,
726   Aeolian Res., 3, 43–54, https://doi.org/10.1016/j.aeolia.2011.01.002, 2011.

727   Bullard, J. E., Baddock, M., Bradwell, T., Crusius, J., Darlington, E., Gaiero, D., Gassó, S.,
728   Gisladottir, G., Hodgkins, R., McCulloch, R., McKenna-Neuman, C., Mockford, T., Stewart, H.,
729   and Thorsteinsson, T.: High-latitude dust in the Earth system, Rev. Geophys., 54, 447–485,
730   https://doi.org/10.1002/2016RG000518, 2016.

731   Creamean, J. M., Kirpes, R. M., Pratt, K. A., Spada, N. J., Maahn, M., de Boer, G., Schnell, R.
732   C., and China, S.: Marine and terrestrial influences on ice nucleating particles during continuous
733   springtime measurements in an Arctic oilfield location, Atmos. Chem. Phys., 18, 18023–18042,
734   https://doi.org/10.5194/acp-18-18023-2018, 2018.

735   Creamean, J. M., Hill, T. C. J., DeMott, P. J., Uetake, J., Kreidenweis, S., and Douglas, T. A.:
736   Thawing permafrost: an overlooked source of seeds for Arctic cloud formation, Environ. Res.
737   Lett., 15, 084022, https://doi.org/10.1088/1748-9326/ab87d3, 2020.

738   Crusius, J., Schroth, A. W., Gassó, S., Moy, C. M., Levy, R. C., and Gatica, M.: Glacial flour
739   dust storms in the Gulf of Alaska: Hydrologic and meteorological controls and their importance
740   as a source of bioavailable iron, Geophys. Res. Lett., 38, L06602,
741   https://doi.org/10.1029/2010GL046573, 2011.

742   Dagsson-Waldhauserova, P., Arnalds, O., and Olafsson, H.: Long-term variability of dust events
743   in Iceland (1949–2011), Atmos. Chem. Phys., 14, 13411–13422, https://doi.org/10.5194/acp-14-
744   13411-2014, 2014.

745   DeMott, P. J., Sassen, K., Poellot, M. R., Baumgardner, D., Rogers, D. C., Brooks, S. D., Prenni,
746   A. J., and Kreidenweis, S. M.: African dust aerosols as atmospheric ice nuclei, Geophys. Res.
747   Lett., 30(14), 1732, https://doi.org/10.1029/2003GL017410, 2003.

748   DeMott, P. J., Prenni, A. J., Liu, X., Kreidenweis, S. M., Petters, M. D., Twohy, C. H.,
749   Richardson, M. S., Eidhammer, T., and Rogers, D. C.: Predicting global atmospheric ice nuclei
750   distributions and their impacts on climate, Proc. Natl. Acad. Sci. U.S.A., 107(25), 11217–11222,
751   https://doi.org/10.1073/pnas.0910818107, 2010.

752   DeMott, P. J., Prenni, A. J., McMeeking, G. R., Sullivan, R. C., Petters, M. D., Tobo, Y.,
753   Niemand, M., Möhler, O., Snider, J. R., Wang, Z., and Kreidenweis, S. M.: Integrating
754   laboratory and field data to quantify the immersion freezing ice nucleation activity of mineral
755   dust particles, Atmos. Chem. Phys., 15, 393–409, https://doi.org/10.5194/acp-15-393-2015, 2015.

756   Dong, X., Xi, B., Crosby, K., Long, C. N., Stone, R. S., and Shupe, M. D.: A 10 year
757   climatology of Arctic cloud fraction and radiative forcing at Barrow, Alaska, J. Geophys. Res.
758   Atmos., 115, D17212, https://doi.org/10.1029/2009JD013489, 2010.

759 Dörnbrack, A., Stachlewska, I. S., Ritter, C., and Neuber, R.: Aerosol distribution around
760 Svalbard during intense easterly winds, Atmos. Chem. Phys., 10, 1473–1490,
761 https://doi.org/10.5194/acp-10-1473-2010, 2010.

762 Fenn, R. W. and Weickmann, H. K.: Some results of aerosol measurements, Geofisica Pura e
763 Applicata, 42, 53–61, https://doi.org/10.1007/BF02113389, 1959.

764 Gettelman, A. and Morrison, H.: Advanced two-moment bulk microphysics for global models.
765 Part I: off-line tests and comparison with other schemes, J. Clim., 28, 1268–1287,
766 https://doi.org/10.1175/JCLI-D-14-00102.1, 2015.

767 Ghan, S. J. and Zaveri, R. A.: Parameterization of optical properties for hydrated internally
768 mixed aerosol, J. Geophys. Res., 112, D10201, https://doi.org/10.1029/2006JD007927, 2007.

769 Ginoux, P., Chin, M., Tegen, I., Prospero, J. M., Holben, B., Dubovik, O., and Lin, S.-J.: Sources
770 and distributions of dust aerosols simulated with the GOCART model, J. Geophys. Res., 106,
771 20255–20273, https://doi.org/10.1029/2000JD000053, 2001.

772 Golaz, J.-C., Larson, V. E., and Cotton, W. R.: A PDF-based model for boundary layer clouds.
773 Part I: Method and model description, J. Atmos. Sci., 59, 3540-3551,
774 https://doi.org/10.1175/1520-0469(2002)059<3540:APBMFB>2.0.CO;2, 2002.

775 Groot Zwaaftink, C. D., Grythe, H., Skov, H., and Stohl, A.: Substantial contribution of northern
776 high-latitude sources to mineral dust in the Arctic, J. Geophys. Res. Atmos., 121, 13678-13697,
777 https://doi.org/10.1002/2016JD025482, 2016.

778 Hiranuma, N., Brooks, S. D., Moffet, R. C., Glen, A., Laskin, A., Gilles, M. K.m Liu, P.,
779 Macdonald, A. M., Strapp, J. W., McFarquhar, G. M: Chemical characterization of individual
780 particles and residuals of cloud droplets and ice crystals collected on board research aircraft in
781 the ISDAC 2008 study, J. Geophys. Res. Atmos., 118, 6564-6579,
782 https://doi.org/10.1002/jgrd.50484, 2013.

783 Hofer, S., Tedstone, A. J., Fettweis, X., and Bamber, J. L.: Cloud microphysics and circulation
784 anomalies control differences in future Greenland melt, Nat. Clim. Chang., 9, 523–528,
785 https://doi.org/10.1038/s41558-019-0507-8, 2019.

786 Holben, B. N., Eck, T. F., Slutsker, I., Tanré, D., Buis, J. P., Setzer, A., Vermote, E., Reagan, J.
787 A., Kaufman, Y. J., Nakajima, T., Lavenu, F., Jankowiak, I., and Smirnov, A.: AERONET—A
788 Federated Instrument Network and Data Archive for Aerosol Characterization, Remote Sens.
789 Environ., 66, 1–16, https://doi.org/10.1016/S0034-4257(98)00031-5, 1998.

790 Hoose, C. and Möhler, O.: Heterogeneous ice nucleation on atmospheric aerosols: a review of
791 results from laboratory experiments, Atmos. Chem. Phys., 12, 9817–9854,
792 https://doi.org/10.5194/acp-12-9817-2012, 2012.

793 Huang, Z., Huang, J., Hayasaka, T., Wang, S., Zhou, T., and Jin, H.: Short-cut transport path for
794 Asian dust directly to the Arctic: a case study, Environ. Res. Lett., 10, 114018,
795 https://doi.org/10.1088/1748-9326/10/11/114018, 2015.

Huneeus, N., Schulz, M., Balkanski, Y., Griesfeller, J., Prospero, J., Kinne, S., Bauer, S., Boucher, O., Chin, M., Dentener, F., Diehl, T., Easter, R., Fillmore, D., Ghan, S., Ginoux, P., Grini, A., Horowitz, L., Koch, D., Krol, M. C., Landing, W., Liu, X., Mahowald, N., Miller, R., Morcrette, J.-J., Myhre, G., Penner, J., Perlwitz, J., Stier, P., Takemura, T., and Zender, C. S.: Global dust model intercomparison in AeroCom phase I, Atmos. Chem. Phys., 11, 7781–7816, https://doi.org/10.5194/acp-11-7781-2011, 2011.

Irish, V. E., Hanna, S. J., Willis, M. D., China, S., Thomas, J. L., Wentzell, J. J. B., Cirisan, A., Si, M., Leaitch, W. R., Murphy, J. G., Abbatt, J. P. D., Laskin, A., Girard, E., and Bertram, A. K.: Ice nucleating particles in the marine boundary layer in the Canadian Arctic during summer 2014, Atmos. Chem. Phys., 19, 1027–1039, https://doi.org/10.5194/acp-19-1027-2019, 2019.

Jacob, D. J., Crawford, J. H., Maring, H., Clarke, A. D., Dibb, J. E., Emmons, L. K., Ferrare, R. A., Hostetler, C. A., Russell, P. B., Singh, H. B., Thompson, A. M., Shaw, G. E., McCauley, E., Pederson, J. R., and Fisher, J. A.: The Arctic Research of the Composition of the Troposphere from Aircraft and Satellites (ARCTAS) mission: design, execution, and first results, Atmos. Chem. Phys., 10, 5191–5212, https://doi.org/10.5194/acp-10-5191-2010, 2010.

Kato, S., Rose, F. G., Rutan, D. A., Thorsen, T. E., Loeb, N. G., Doelling, D. R., Huang, X., Smith, W. L., Su, W., and Ham, S.-H.: Surface irradiances of Edition 4.0 Clouds and the Earth's Radiant Energy System (CERES) Energy Balanced and Filled (EBAF) data product, J. Climate, 31, 4501-4527, https://doi.org/10.1175/JCLI-D-17-0523.1, 2018.

Khanal, S., Wang, Z., and French, J. R.: Improving middle and high latitude cloud liquid water path measurements from MODIS, Atmos. Res., 243. 105033. https://doi.org/10.1016/j.atmosres.2020.105033, 2020.

Kinne, S., Schulz, M., Textor, C., Guibert, S., Balkanski, Y., Bauer, S. E., Berntsen, T., Berglen, T. F., Boucher, O., Chin, M., Collins, W., Dentener, F., Diehl, T., Easter, R., Feichter, J., Fillmore, D., Ghan, S., Ginoux, P., Gong, S., Grini, A., Hendricks, J., Herzog, M., Horowitz, L., Isaksen, I., Iversen, T., Kirkevåg, A., Kloster, S., Koch, D., Kristjansson, J. E., Krol, M., Lauer, A., Lamarque, J. F., Lesins, G., Liu, X., Lohmann, U., Montanaro, V., Myhre, G., Penner, J., Pitari, G., Reddy, S., Seland, O., Stier, P., Takemura, T., and Tie, X.: An AeroCom initial assessment – optical properties in aerosol component modules of global models, Atmos. Chem. Phys., 6, 1815–1834, https://doi.org/10.5194/acp-6-1815-2006, 2006.

Kohfeld, K. E. and Harrison, S. P.: DIRTMAP: the geological record of dust, Earth-Sci. Rev., 54, 81–114, https://doi.org/10.1016/S0012-8252(01)00042-3, 2001.

Kok, J. F.: A scaling theory for the size distribution of emitted dust aerosols suggests climate models underestimate the size of the global dust cycle, Proc. Natl. Acad. Sci. U.S.A., 108(3), 1016–1021, https://doi.org/10.1073/pnas.1014798108, 2011.

Kok, J. F., Mahowald, N. M., Fratini, G., Gillies, J. A., Ishizuka, M., Leys, J. F., Mikami, M., Park, M.-S., Park, S.-U., Van Pelt, R. S., and Zobeck, T. M.: An improved dust emission model – Part 1: Model description and comparison against measurements, Atmos. Chem. Phys., 14, 13023–13041, https://doi.org/10.5194/acp-14-13023-2014, 2014a.

835 Kok, J. F., Albani, S., Mahowald, N. M., and Ward, D. S.: An improved dust emission model –
836 Part 2: Evaluation in the Community Earth System Model, with implications for the use of dust
837 source functions, Atmos. Chem. Phys., 14, 13043–13061, https://doi.org/10.5194/acp-14-13043-
838 2014, 2014b.

839 Kok, J. F., Ridley, D. A., Zhou, Q., Miller, R. L., Zhao, C., Heald, C. L., Ward, D. S., Albani, S.,
840 and Haustein, K.: Smaller desert dust cooling effect estimated from analysis of dust size and
841 abundance, Nat. Geosci., 10, 274–278, https://doi.org/10.1038/ngeo2912, 2017.

842 Kulkarni, G., Sanders, C., Zhang, K., Liu, X., and Zhao, C.: Ice nucleation of bare and sulfuric
843 acid-coated mineral dust particles and implication for cloud properties, 119, 9993–10011,
844 https://doi.org/10.1002/2014JD021567, 2014.

845 Larson, V. E., Golaz, J.-C., and Cotton, W. R.: Small-Scale and Mesoscale Variability in Cloudy
846 Boundary Layers: Joint Probability Density Functions, J. Atmos. Sci., 59, 3519-3539,
847 https://doi.org/10.1175/1520-0469(2002)059<3519:SSAMVI>2.0.CO;2, 2002.

848 Liu, X., Xie, S., Boyle, J., Klein, S. A., Shi, X., Wang, Z., Lin, W., Ghan, S. J., Earle, M., Liu, P.
849 S. K., and Zelenyuk, A.: Testing cloud microphysics parameterizations in NCAR CAM5 with
850 ISDAC and M-PACE observations, J. Geophys. Res., 116, D00T11,
851 https://doi.org/10.1029/2011JD015889, 2011.

852 Liu, X., Ma, P.-L., Wang, H., Tilmes, S., Singh, B., Easter, R. C., Ghan, S. J., and Rasch, P. J.:
853 Description and evaluation of a new four-mode version of the Modal Aerosol Module (MAM4)
854 within version 5.3 of the Community Atmosphere Model, Geosci. Model Dev., 9, 505–522,
855 https://doi.org/10.5194/gmd-9-505-2016, 2016.

856 Loeb, N. G., Doelling, D. R., Wang, H., Su, W., Nguyen, C., Corbett, J. G., Liang, L., Mitrescu,
857 C., Rose, F. G., and Kato, S.: Clouds and the Earth's Radiant Energy System (CERES) Energy
858 Balanced and Filled (EBAF) Top-of-Atmosphere (TOA) Edition-4.0 Data Product. J. Climate,
859 31, 895-918, https://doi.org/ 10.1175/JCLI-D-17-0208.1, 2018.

860 Luo, C., Mahowald, N. M., and Corral, J. del: Sensitivity study of meteorological parameters on
861 mineral aerosol mobilization, transport, and distribution, J. Geophys. Res., 108, 4447,
862 https://doi.org/10.1029/2003JD003483, 2003.

863 Luo, T., Wang, Z., Ferrare, R. A., Hostetler, C. A., Yuan, R., and Zhang, D.: Vertically resolved
864 separation of dust and other aerosol types by a new lidar depolarization method, Opt. Express, 23,
865 14095-14107, https://doi.org/10.1364/OE.23.014095, 2015a.

866 Luo, T., Wang, Z., Zhang, D., Liu, X., Wang, Y., and Yuan, R.: Global dust distribution from
867 improved thin dust layer detection using A-train satellite lidar observations, Geophys. Res. Lett.,
868 42, 620–628, https://doi.org/10.1002/2014GL062111, 2015b.

869 Maenhaut, W., Fernandez-Jimenez, M.-T., Rajta, I., Dubtsov, S., Meixner, F. X., Andreae, M. O.,
870 Torr, S., Hargrove, J. W., Chimanga, P., and Mlambo, J.: Long-term aerosol composi- tion
871 measraments and source apportionment at Rukomechi, Zim- babwe, J. Aerosol Sci., 31(Suppl. 1),
872 S469–S470, 2000a.

873 Maenhaut, W., Fernandez-Jimenez, M.-T., Vanderzalm, J. L., Hooper, B. M., Hooper, M. A.,
874 and Tapper, N. J.: Aerosol com- position at Jabiru, Australia and impact of biomass burning, J.
875 Aerosol Sci., 31(Suppl. 1), S745–S746, 2000b.

876 Mahowald, N. M., Engelstaedter, S., Luo, C., Sealy, A., Artaxo, P., Benitez-Nelson, C., Bonnet,
877 S., Chen, Y., Chuang, P. Y., Cohen, D. D., Dulac, F., Herut, B., Johansen, A. M., Kubilay, N.,
878 Losno, R., Maenhaut, W., Paytan, A., Prospero, J. M., Shank, L. M., and Siefert, R. L.:
879 Atmospheric iron deposition: global distribution, variability, and human perturbations, Ann. Rev.
880 Mar. Sci., 1, 245–278, https://doi.org/10.1146/annurev.marine.010908.163727, 2009.

881 Mason, R. H., Si, M., Chou, C., Irish, V. E., Dickie, R., Elizondo, P., Wong, R., Brintnell, M.,
882 Elsasser, M., Lassar, W. M., Pierce, K. M., Leaitch, W. R., MacDonald, A. M., Platt, A., Toom-
883 Sauntry, D., Sarda-Estève, R., Schiller, C. L., Suski, K. J., Hill, T. C. J., Abbatt, J. P. D.,
884 Huffman, J. A., DeMott, P. J., and Bertram, A. K.: Size-resolved measurements of ice-nucleating
885 particles at six locations in North America and one in Europe, Atmos. Chem. Phys., 16, 1637–
886 1651, https://doi.org/10.5194/acp-16-1637-2016, 2016.

887 McCluskey, C. S., Ovadnevaite, J., Rinaldi, M., Atkinson, J., Belosi, F., Ceburnis, D., Marullo,
888 S., Hill, T. C. J., Lohmann, U., Kanji, Z. A., O'Dowd, C., Kreidenweis, S. M., and DeMott, P. J.:
889 Marine and terrestrial organic ice-nucleating particles in pristine marine to continentally
890 influenced Northeast Atlantic air masses, J. Geophys. Res. Atmos., 123, 6196–6212,
891 https://doi.org/10.1029/2017JD028033, 2018.

892 McFarquhar, G. M., Ghan, S., Verlinde, J., Korolev, A., Strapp, J. W., Schmid, B., Tomlinson, J.
893 M., Wolde, M., Brooks, S. D., Cziczo, D., Dubey, M. K., Fan, J., Flynn, C., Gultepe, I., Hubbe,
894 J., Gilles, M. K., Laskin, A., Lawson, P., Leaitch, W. R., Liu, P., Liu, X., Lubin, D., Mazzoleni,
895 C., Macdonald, A.-M., Moffet, R. C., Morrison, H., Ovchinnikov, M., Shupe, M. D., Turner, D.
896 D., Xie, S., Zelenyuk, A., Bae, K., Freer, M., and Glen, A.: Indirect and Semi-direct Aerosol
897 Campaign: The Impact of Arctic Aerosols on Clouds, Bull. Amer. Meteor. Soc., 92, 183–201,
898 https://doi.org/10.1175/2010BAMS2935.1, 2011.

899 Morrison, H., de Boer, G., Feingold, G., Harrington, J., Shupe, M. D., and Sulia, K.: Resilience
900 of   persistent   Arctic   mixed-phase   clouds,   Nat.   Geosci.,   5,   11–17,
901 https://doi.org/10.1038/ngeo1332, 2012.

902 Murray, B. J., O'Sullivan, D., Atkinson, J. D., and Webb, M. E.: Ice nucleation by particles
903 immersed   in   supercooled   cloud   droplets,   Chem.   Soc.   Rev.,   41,   6519-6554,
904 https://doi.org/10.1039/c2cs35200a, 2012.

905 Paramonov, M., David, R. O., Kretzschmar, R., and Kanji, Z. A.: A laboratory investigation of
906 the ice nucleation efficiency of three types of mineral and soil dust, Atmos. Chem. Phys., 18,
907 16515–16536, https://doi.org/10.5194/acp-18-16515-2018, 2018.

908 Prenni, A. J., Harrington, J. Y., Tjernström, M., DeMott, P. J., Avramov, A., Long, C. N.,
909 Kreidenweis, S. M., Olsson, P. Q., and Verlinde, J.: Can ice-nucleating aerosols affect Arctic
910 seasonal climate?, Bull. Amer. Meteor. Soc., 88, 541–550, https://doi.org/10.1175/BAMS-88-4-
911 541, 2007.

Prenni, A. J., Demott, P. J., Rogers, D. C., Kreidenweis, S. M., Mcfarquhar, G. M., Zhang, G., and Poellot, M. R.: Ice nuclei characteristics from M-PACE and their relation to ice formation in clouds, Tellus B, 61, 436–448, https://doi.org/10.1111/j.1600-0889.2009.00415.x, 2009.

Prospero, J. M.: The Atmospheric Transport of Particles to the Ocean, in: Particle Flux in the Ocean, edited by: Ittekkot, V., Sch¨afer, P., Honjo, S., and Depetris, P. J., John Wiley & Sons Ltd., New York, 1996.

Prospero, J. M., Bullard, J. E., and Hodgkins, R.: High-Latitude Dust Over the North Atlantic: Inputs from Icelandic Proglacial Dust Storms, Science, 335, 1078–1082, https://doi.org/10.1126/science.1217447, 2012.

Prospero, J. M., Uematsu, M., and Savoie, D. L.: Mineral aerosol transport to the Pacific Ocean, edited by: Riley, J. P., 187–218, Academic Press, New York, 1989.

Rasch, P. J., Xie, S., Ma, P. -L., Lin, W., Wang, H., Tang, Q., Burrows, S. M., Caldwell, P., Zhang, K., Easter, R. C., Cameron-Smith, P., Singh, B., Wan, H., Golaz, J. -C., Harrop, B. E., Roesler, E., Bacmeister, J., Larson, V. E., Evans, K. J., Qian, Y., Taylor, M., Leung, L. R., Zhang, Y., Brent, L., Branstetter, M., Hannay, C., Mahajan, S., Mametjanov, A., Neale, R., Richter, J. H., Yoon, J. -H., Zender, C. S., Bader, D., Flanner, M., Foucar, J. G., Jacob, R., Keen, N., Klein, S. A., Liu, X., Salinger, A. G., Shrivastava, M., and Yang, Y.: An overview of the atmospheric component of the Energy Exascale Earth System Model, J. Adv. Model. Earth Syst., 11, 2377–2411, https://doi.org/10.1029/2019MS001629, 2019.

Ridley, D. A., Heald, C. L., Kok, J. F., and Zhao, C.: An observationally constrained estimate of global dust aerosol optical depth, Atmos. Chem. Phys., 16, 15097–15117, https://doi.org/10.5194/acp-16-15097-2016, 2016.

Sanchez-Marroquin, A., Arnalds, O., Baustian-Dorsi, K. J., Browse, J., Dagsson-Waldhauserova, P., Harrison, A. D., Maters, E. C., Pringle, K. J., Vergara-Temprado, J., Burke, I. T., McQuaid, J. B., Carslaw, K. S., and Murray, B. J.: Iceland is an episodic source of atmospheric ice-nucleating particles relevant for mixed-phase clouds, Sci. Adv., 6, eaba8137, https://doi.org/10.1126/sciadv.aba8137, 2020.

Schill, G. P., DeMott, P. J., Emerson, E. W., Rauker, A. M. C., Kodros, J. K., Suski, K. J., Hill, T. C. J., Levin, E. J. T., Pierce, J. R., Farmer, D. K., and Kreidenweis, S. M.: The contribution of black carbon to global ice nucleating particle concentrations relevant to mixed-phase clouds, Proc. Natl. Acad. Sci. U.S.A., 117, 22705–22711, https://doi.org/10.1073/pnas.2001674117, 2020.

Schweiger, A. J., Lindsay, R. W., Vavrus, S., and Francis, J. A.: Relationships between Arctic sea ice and clouds dusting autumn, J. Clim., 21, 4799-4810, https://doi.org/10.1175/2008JCLI2156.1

Shao, Y., Wyrwoll, K.-H., Chappell, A., Huang, J., Lin, Z., McTainsh, G. H., Mikami, M., Tanaka, T. Y., Wang, X., and Yoon, S.: Dust cycle: An emerging core theme in Earth system science, Aeolian Res., 2, 181–204, https://doi.org/10.1016/j.aeolia.2011.02.001, 2011.

Shi, Y. and Liu, X.: Dust Radiative Effects on Climate by Glaciating Mixed-Phase Clouds, Geophys. Res. Lett., 46, 6128–6137, https://doi.org/10.1029/2019GL082504, 2019.

Shupe, M. D. and Intrieri, J. M.: Cloud Radiative Forcing of the Arctic Surface: The Influence of Cloud Properties, Surface Albedo, and Solar Zenith Angle, J. Clim., 17, 616–628, https://doi.org/10.1175/1520-0442(2004)017<0616:CRFOTA>2.0.CO;2, 2004.

Si, M., Evoy, E., Yun, J., Xi, Y., Hanna, S. J., Chivulescu, A., Rawlings, K., Veber, D., Platt, A., Kunkel, D., Hoor, P., Sharma, S., Leaitch, W. R., and Bertram, A. K.: Concentrations, composition, and sources of ice-nucleating particles in the Canadian High Arctic during spring 2016, Atmos. Chem. Phys., 19, 3007–3024, https://doi.org/10.5194/acp-19-3007-2019, 2019.

Sirois, A., and Barrie, L. A.: Arctic lower tropospheric aerosol trends and composition at Alert, Canada: 1980-1995, J. Geophys. Res. Atmos., 104, 11599-11618, https://doi.org/10.1029/1999JD900077, 1999.

Smirnov, A., Holben, B. N., Eck, T. F., Dubovik, O., and Slutsker, I.: Cloud screening and quality control algorithms for the AERONET database, Remote Sens. Environ., 73, 337–349, https://doi.org/10.1016/S0034-4257(00)00109-7, 2000.

Stohl, A.: Characteristics of atmospheric transport into the Arctic troposphere, J. Geophys. Res., 111, D11306, https://doi.org/10.1029/2005JD006888, 2006.

Stone, R., Anderson, G., Andrews, E., Dutton, E., Harris, J., Shettle, E., Berk, A.: Asian dust signatures at Barrow: observed and simulated. Incursions and impact of Asian dust over Northern Alaska, Workshop on Remote Sensing of Atmospheric Aerosols, IEEE Workshop on Remote Sensing of Atmospheric Aerosols, 74-79, https://doi.org/10.1109/AERSOL.2005.1494152, 2005.

Tan, I. and Storelvmo, T.: Sensitivity study on the influence of cloud microphysical parameters on mixed-phase cloud thermodynamic phase partitioning in CAM5, J. Atmos. Sci., 73, 709-728, https://doi.org/10.1175/JAS-D-15-0152.1, 2016.

Tan, I. and Storelvmo, T.: Evidence of Strong Contributions from Mixed-Phase Clouds to Arctic Climate Change, Geophys. Res. Lett., 46, 2894–2902, https://doi.org/10.1029/2018GL081871, 2019.

Tanaka, T. Y. and Chiba, M.: A numerical study of the contributions of dust source regions to the global dust budget, Glob. Planet. Change, 52, 88–104, https://doi.org/10.1016/j.gloplacha.2006.02.002, 2006.

Tegen, I., Harrison, S. P., Kohfeld, K., Prentice, I. C., Coe, M., and Heimann, M.: Impact of vegetation and preferential source areas on global dust aerosol: Results from a model study, J. Geophys. Res. Atmos., 107, AAC 14-1-AAC 14-27, https://doi.org/10.1029/2001JD000963, 2002.

Tobo, Y., Adachi, K., DeMott, P. J., Hill, T. C. J., Hamilton, D. S., Mahowald, N. M., Nagatsuka, N., Ohata, S., Uetake, J., Kondo, Y., and Koike, M.: Glacially sourced dust as a potentially

987 significant source of ice nucleating particles, Nat. Geosci., 12, 253–258,
988 https://doi.org/10.1038/s41561-019-0314-x, 2019.

989 Vali, G.: Nucleation terminology, Bull. Am. Meteorol. Soc., 66, 1426–1427, 1985.

990 Vali, G., DeMott, P. J., Möhler, O., and Whale, T. F.: Technical Note: A proposal for ice
991 nucleation terminology, Atmos. Chem. Phys., 15, 10263–10270, https://doi.org/10.5194/acp-15-
992 10263-2015, 2015.

993 VanCuren, R. A., Cahill, T., Burkhart, J., Barnes, D., Zhao, Y., Perry, K., Cliff, S., and
994 McConnell, J.: Aerosols and their sources at Summit Greenland – First results of continuous
995 size- and time-resolved sampling, Atmos. Environ., 52, 82–97,
996 https://doi.org/10.1016/j.atmosenv.2011.10.047, 2012.

997 Wang, H., Rasch, P. J., Easter, R. C., Singh, B., Zhang, R., Ma, P.-L., Qian, Y., Ghan, S. J., and
998 Beagley, N.: Using an explicit emission tagging method in global modeling of source-receptor
999 relationships for black carbon in the Arctic: Variations, sources, and transport pathways, J.
1000 Geophys. Res. Atmos., 119, 12888-12909, https://doi.org/10.1002/2014JD022297, 2014.

1001 Wang, H., Easter, R. C., Zhang, R., Ma, P.-L., Singh, B., Zhang, K., Ganguly, D., Rasch, P. J.,
1002 Burrows, S. M., Ghan, S. J., Lou, S., Qian, Y., Yang, Y., Feng, Y., Flanner, M., Leung, L. R.,
1003 Liu, X., Shrivastava, M., Sun, J., Tang, Q., Xie, S., and Yoon, J.: Aerosols in the E3SM Version
1004 1: New Developments and Their Impacts on Radiative Forcing, J. Adv. Model. Earth Syst., 12,
1005 e2019MS001851, https://doi.org/10.1029/2019MS001851, 2020.

1006 Wang, Y., Liu, X., Hoose, C., and Wang, B.: Different contact angle distributions for
1007 heterogeneous ice nucleation in the Community Atmospheric Model version 5, Atmos. Chem.
1008 Phys., 14, 10411–10430, https://doi.org/10.5194/acp-14-10411-2014, 2014.

1009 Westbrook, C. D. and Illingworth, A. J.: The formation of ice in a long-lived supercooled layer
1010 cloud: Ice Formation in Altocumulus, Q. J. R. Meteorol. Soc., 139, 2209–2221,
1011 https://doi.org/10.1002/qj.2096, 2013.

1012 Wilson, T. W., Ladino, L. A., Alpert, P. A., Breckels, M. N., Brooks, I. M., Browse, J., Burrows,
1013 S. M., Carslaw, K. S., Huffman, J. A., Judd, C., Kilthau, W. P., Mason, R. H., McFiggans, G.,
1014 Miller, L. A., Nájera, J. J., Polishchuk, E., Rae, S., Schiller, C. L., Si, M., Vergara-Temprado, J.,
1015 Whale, T. F., Wong, J. P. S., Wurl, O., Yakobi-Hancock, J. D., Abbatt, J. P. D., Aller, J. Y.,
1016 Bertram, A. K., Knopf, D. A., and Murray, B. J.: A marine biogenic source of atmospheric ice-
1017 nucleating particles, Nature, 525, 234–238, https://doi.org/10.1038/nature14986, 2015.

1018 Winker, D. M., Tackett, J. L., Getzewich, B. J., Liu, Z., Vaughan, M. A., and Rogers, R. R.: The
1019 global 3-D distribution of tropospheric aerosols as characterized by CALIOP, Atmos. Chem.
1020 Phys., 13, 3345–3361, https://doi.org/10.5194/acp-13-3345-2013, 2013.

1021 Wu, M., Liu, X., Yu, H., Wang, H., Shi, Y., Yang, K., Darmenov, A., Wu, C., Wang, Z., Luo, T.,
1022 Feng, Y., and Ke, Z.: Understanding processes that control dust spatial distributions with global
1023 climate models and satellite observations, Atmos. Chem. Phys., 20, 13835–13855,
1024 https://doi.org/10.5194/acp-20-13835-2020, 2020.

1025 Yang, K., Wang, Z., Luo, T., and Liu, X.: Upper Troposphere Dust Belt formation processes
1026 vary seasonally and spatially in the Northern Hemisphere, Commun. Earth Environ., accepted,
1027 2022.

1028 Yang, Y., Wang, H., Smith, S. J., Easter, R., Ma, P.-L., Qian, Y., Yu, H., Li, C., and Rasch, P. J.:
1029 Global source attribution of sulfate concentration and direct and indirect radiative forcing, Atmos.
1030 Chem. Phys., 17, 8903–8922, https://doi.org/10.5194/acp-17-8903-2017, 2017a.

1031 Yang, Y., Wang, H., Smith, S. J., Ma, P.-L., and Rasch, P. J.: Source attribution of black carbon
1032 and its direct radiative forcing in China, Atmos. Chem. Phys., 17, 4319–4336,
1033 https://doi.org/10.5194/acp-17-4319-2017, 2017b.

1034 Yang, Y., Wang, H., Smith, S. J., Zhang, R., Lou, S., Yu, H., Li, C., and Rasch, P. J.: Source
1035 Apportionments of Aerosols and Their Direct Radiative Forcing and Long-Term Trends Over
1036 Continental United States, Earth's Future, 6, 793–808, https://doi.org/10.1029/2018EF000859,
1037 2018.

1038 Zender, C. S., Bian, H., and Newman, D.: Mineral Dust Entrainment and Deposition (DEAD)
1039 model: Description and 1990s dust climatology, J. Geophys. Res., 108, 4416,
1040 https://doi.org/10.1029/2002JD002775, 2003.

1041 Zhang, G. J. and McFarlane, N. A.: Sensitivity of climate simulations to the parameterization of
1042 cumulus convection in the Canadian climate centre general circulation model, Atmos.-Ocean, 33,
1043 407–446, https://doi.org/10.1080/07055900.1995.9649539, 1995.

1044 Zhang, K., Wan, H., Liu, X., Ghan, S. J., Kooperman, G. J., Ma, P.-L., Rasch, P. J., Neubauer,
1045 D., and Lohmann, U.: Technical Note: On the use of nudging for aerosol–climate model
1046 intercomparison studies, Atmos. Chem. Phys., 14, 8631–8645, https://doi.org/10.5194/acp-14-
1047 8631-2014, 2014.

1048 Zhang, M., Liu, X., Diao, M., D'Alessandro, J. J., Wang, Y., Wu, C., Zhang, D., Wang, Z., and
1049 Xie, S.: Impacts of representing heterogeneous distribution of cloud liquid and ice on phase
1050 partitioning of Arctic mixed-phase clouds with NCAR CAM5, J. Geophys. Res. Atmos., 124,
1051 13071–13090, https://doi.org/10.1029/2019JD030502, 2019.

1052 Zhang, M., Xie, S., Liu, X., Lin, W., Zhang, K., Ma, H.-Y., Zheng, X., and Zhang, Y.: Toward
1053 understanding the simulated phase partitioning of Arctic single-layer mixed-phase clouds in
1054 E3SM, Earth Space Sci., 7, e2020EA001125, https://doi.org/10.1029/2020EA001125, 2020.

1055 Zhang, Y., Xie, S., Lin, W., Klein, S. A., Zelinka, M., Ma, P., Rasch, P. J., Qian, Y., Tang, Q.,
1056 and Ma, H.: Evaluation of clouds in version 1 of the E3SM atmosphere model with satellite
1057 simulators, J. Adv. Model. Earth Syst., 11, 1253–1268, https://doi.org/10.1029/2018MS001562,
1058 2019.

1059 Zhao, X. and Liu, X.: Global Importance of Secondary Ice Production, Geophys. Res. Lett., 48,
1060 e2021GL092581, https://doi.org/10.1029/2021GL092581, 2021.

1061   Zhao, X., Liu, X., Burrows, S. M., and Shi, Y.: Effects of marine organic aerosols as sources of
1062   immersion-mode ice-nucleating particles on high-latitude mixed-phase clouds, Atmos. Chem.
1063   Phys., 21, 2305–2327, https://doi.org/10.5194/acp-21-2305-2021, 2021a.

1064   Zhao, X., Liu, X., Phillips, V. T. J., and Patade, S.: Impacts of secondary ice production on
1065   Arctic mixed-phase clouds based on ARM observations and CAM6 single-column model
1066   simulations, Atmos. Chem. Phys., 21, 5685–5703, https://doi.org/10.5194/acp-21-5685-2021,
1067   2021b.

1068

1069 **Table 1.** Experiments conducted in this study.

Experiment	Description
CTRL	Control simulation using the CNT parameterization for heterogeneous ice nucleation and Kok et al. (2014a, b) for dust emission parameterization.
noArc	Same as CTRL, but turn off heterogeneous ice nucleation in mixed-phase clouds by HLD.
noNAf	Same as CTRL, but turn off heterogeneous ice nucleation in mixed-phase clouds by North African dust.
noEAs	Same as CTRL, but turn off heterogeneous ice nucleation in mixed-phase clouds by East Asian dust.

1070

1071   **Table 2.** Annual and seasonal mean Arctic (60-90°N) dust burden (mg m^{-2}) from different
1072   sources. The numbers in parentheses are the relative contributions (%) of each source to the total
1073   Arctic dust burden. The total Arctic dust burden is shown in the last row.

	ANN	MAM	JJA	SON	DJF
Arc	2.1 (30.7)	0.3 (3.9)	5.1 (50.4)	2.5 (47.5)	0.5 (14.6)
NAm	0.1 (0.9)	0.1 (1.3)	0.1 (0.6)	0.0 (0.7)	0.0 (1.2)
NAf	1.7 (24.2)	3.7 (41.4)	1.5 (14.4)	0.7 (12.9)	0.9 (26.4)
CAs	0.9 (12.8)	1.1 (12.5)	1.3 (13.0)	0.8 (14.7)	0.3 (10.1)
MSA	0.8 (11.5)	1.6 (17.9)	0.7 (7.0)	0.3 (6.1)	0.6 (17.4)
EAs	1.4 (19.9)	2.0 (23.0)	1.5 (14.7)	0.9 (18.1)	1.0 (30.2)
RoW	0.0 (0.0)	0.0 (0.0)	0.0 (0.0)	0.0 (0.0)	0.0 (0.1)
Total Burden (mg m^{-2})	6.9	8.9	10.2	5.2	3.3

1074

1075   **Table 3.** Summary of the nine Arctic INP measurements used for INP comparisons in Figure 8.

	Location	Time period	Measured platform	Reference	Possible INP source mentioned in literature	INP source attribution from modeling[+]
A	Utqiaġvik	Apr. 2008 (spring)	Aircraft	McFarquhar et al. (2011)	Metallic or composed of dust[*]	LLD (EAs)
B	Alert	Mar. - May 2014 (spring)	Ground-based	Mason et al. (2016)	Not mentioned	LLD (EAs)
C	Alert	Mar. 2016 (spring)	Ground-based	Si et al. (2019)	LLD from Gobi Desert	LLD (EAs)
D	Zeppelin	Mar. 2017 (spring)	Ground-based	Tobo et al. (2019)	Marine organic aerosols	HLD (NEu)
E	Oliktok Point	Mar. - May 2017 (spring)	Ground-based	Creamean et al. (2018)	Dust and primary marine aerosols	LLD (mainly from EAs and some from NAf)
F	Alert	Jun. - Jul. 2014 (summer)	Ground-based	Mason et al. (2016)	Not mentioned	HLD (NCa)
G	Zeppelin	Jul. 2016 (summer)	Ground-based	Tobo et al. (2019)	HLD from Svalbard or other high latitude sources[**]	HLD (NEu)
H	Utqiaġvik	Oct. 2004 (autumn)	Aircraft	Prenni et al. (2007)	Dust and carbonaceous particles	HLD (NCa) and LLD (EAs)
I	South of Iceland	Oct. 2014 (autumn)	Aircraft	Sanchez-Marroquin et al. (2020)	Icelandic dust	Dominated by HLD (GrI), little from LLD (NAf)

1076   [+] The modeling analyses include INP contribution from HLD (using SM20), LLD (using D15),
1077   BC, and SSA. The
1078   [*] Carbonate, black carbon, and organic may also contribute, according to Hiranuma et al. (2013).
1079   [**] The HLD in this campaign is reported to have remarkably high ice nucleating ability, which
1080   may be related to the presence of organic matter.
1081

1082 **Table 4.** Arctic (60-90°N) averaged surface downwelling radiative fluxes and TOA cloud
1083 radiative forcing changes caused by dust INPs originated from local Arctic sources (Arc), North
1084 Africa (NAf), and East Asia (EAs). Units are W m^{-2}.

	ANN			MAM			JJA			SON			DJF		
	SW	LW	Net	SW	LW	Net	SW	LW	Net	SW	LW	Net	SW	LW	Net
Part 1. INP effect on surface downwelling radiative fluxes															
Arc	0.11	-0.36	-0.24	0.27	-0.31	-0.03	0.12	0	0.12	0.04	-0.55	-0.51	0.02	-0.56	-0.54
NAf	0.33	-0.25	0.08	0.78	-0.60	0.19	0.50	0.01	0.51	0.02	-0.03	-0.02	0.03	-0.39	-0.36
EAs	0.35	-0.41	-0.06	0.68	-0.60	0.09	0.59	0.02	0.61	0.08	-0.27	-0.19	0.04	-0.80	-0.76
Part 2. INP effect on TOA cloud radiative forcing															
Arc	0.06	-0.11	-0.05	0.06	-0.07	-0.01	0.14	-0.02	0.12	0.03	-0.23	-0.20	0.01	-0.12	-0.11
NAf	0.20	-0.23	-0.03	0.34	-0.34	0	0.41	-0.18	0.24	0.03	-0.20	-0.16	0.02	-0.23	-0.21
EAs	0.20	-0.24	-0.04	0.22	-0.23	-0.02	0.46	-0.17	0.29	0.09	-0.29	-0.20	0.02	-0.26	-0.24

1085
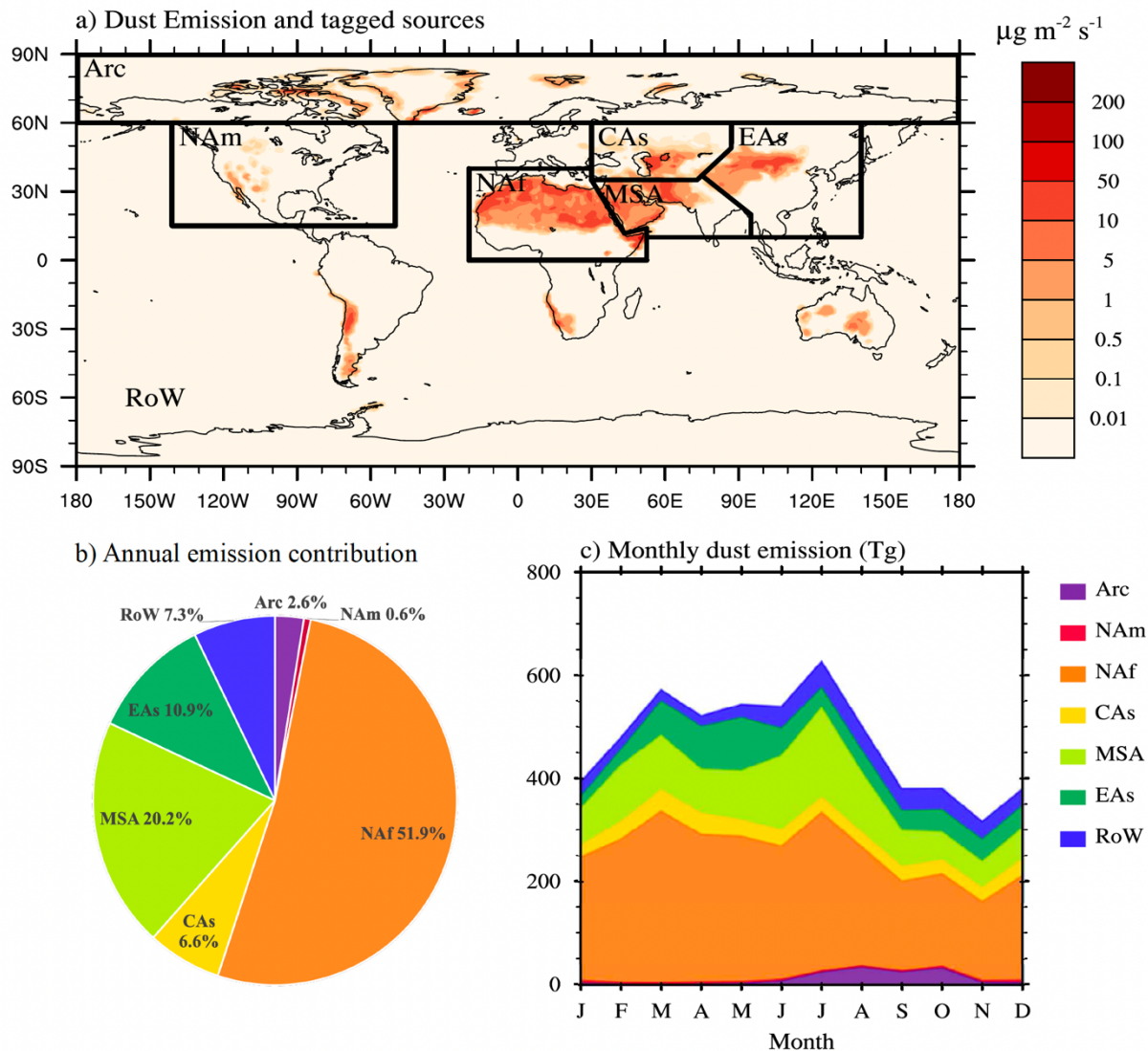
1086

1087   **Figure 1.** a) Simulated global annual mean dust emission with 7 tagged source regions (Arc:
1088   Arctic; NAm: North America; NAf: North Africa; CAs: Central Asia; MSA: Middle East and
1089   South Asia; EAs: East Asia; RoW: Rest of the World). b) The respective percentage
1090   contributions to the global annual mean dust emission from the individual source regions. c)
1091   Seasonal cycle of global dust emission.
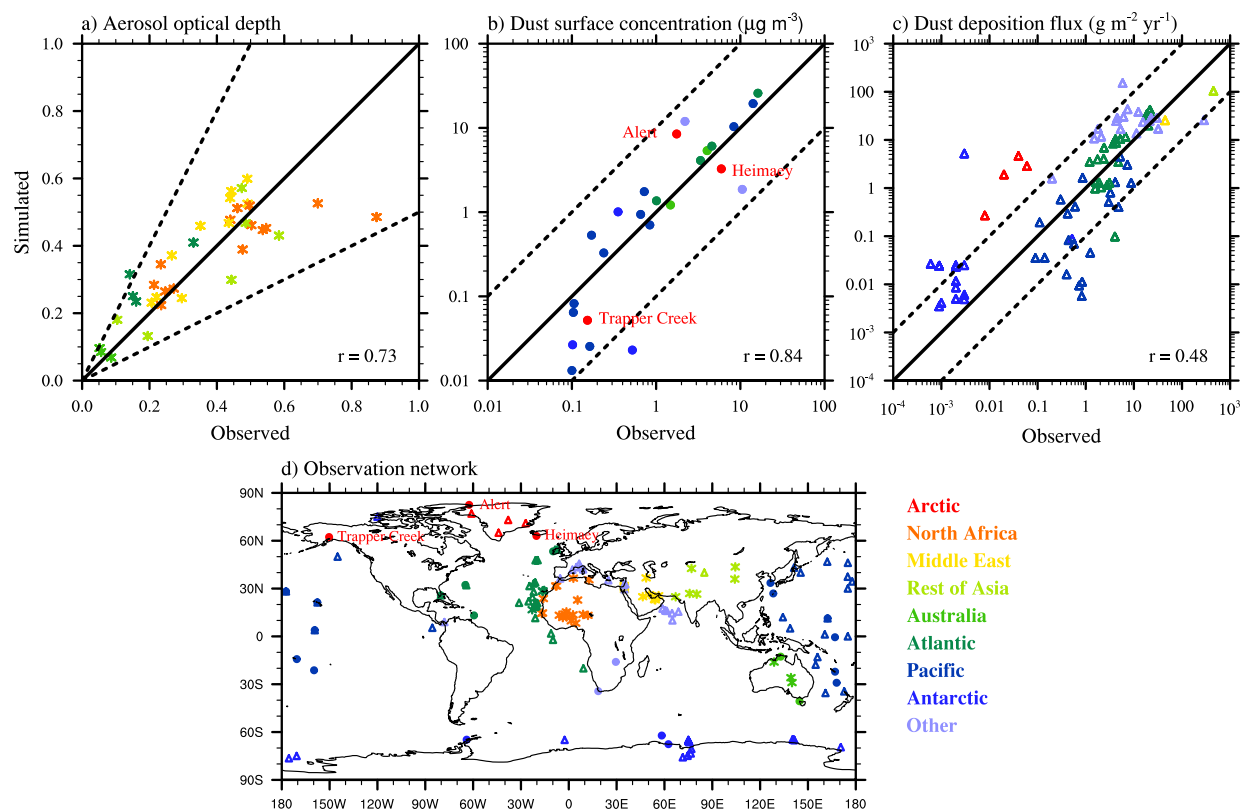
1092

Figure 2. Comparison of observed and simulated a) averaged AOD at 40 dust-dominated stations (stars), b) dust surface concentration at 25 sites (circles), and c) dust deposition flux at 84 sites (triangles). Solid lines represent 1:1 comparison. Dashed lines mark 2 factor of magnitude bias in panel a) and 1 order of magnitude differences in panel b) and c). For each comparison, the correlation coefficient (r) is noted. The AOD data is conducted by AERONET. The dust surface concentration measurements include 20 stations managed by Rosenstiel School of Marine and Atmospheric Science at the University of Miami (Prospero et al., 1989; Prospero, 1996; Arimoto et al., 1995), two Australia stations (Maenhaut et al., 2000a, b), and three Arctic stations (Heimaey (Prospero et al., 2012), Alert (Sirois and Barrie, 1999), and Trapper Creek (IMPROVE)). The deposition fluxes data is a compilation of measurements from Ginoux et al. (2001), Mahowald et al. (2009), and the Dust Indicators and Records in Terrestrial and Marine Paleoenvironments (DIRTMAP) database (Tegen et al., 2002; Kohfeld and Harrison, 2001). Stations are grouped regionally and classified by different colors. The locations of the measurements are shown in panel d).

1107
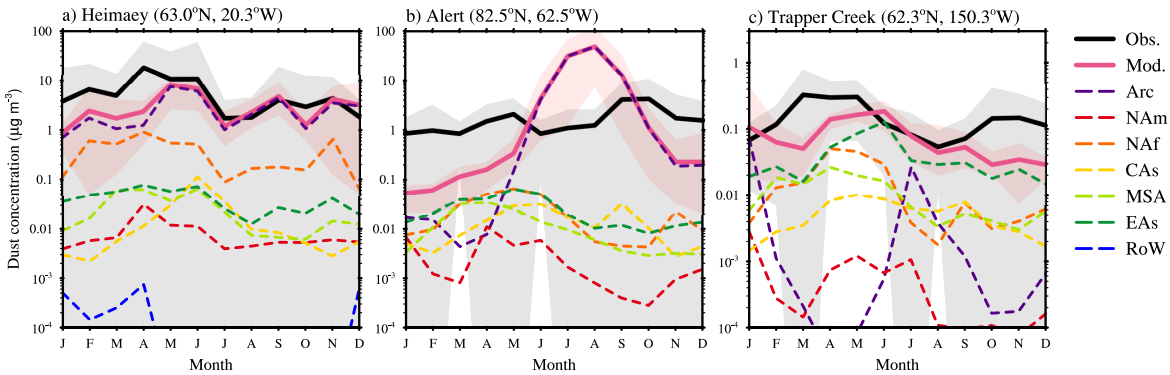
1108

Figure 3. Comparison of measured (black solid line, with gray shade representing standard deviation) and simulated (pink solid line, with pink shade representing year-to-year variability) monthly mean dust surface concentration at three high latitude stations – a) Heimaey, b) Alert, and c) Trapper Creek. The model results are averaged from year 2007 to 2011. Contributions from seven tagged sources are shown by colored dashed lines. The locations of the three stations are shown in Figure 2d. The measurements at Heimaey (Prospero et al., 2012), Alert (Sirois and Barrie, 1999), and Trapper Creek (IMPROVE) are averaged for the years 1997 to 2002, 1980 to 1995, and 2007 to 2011, respectively. The dust concentrations at Trapper Creek only include particles with diameter less than 2.5 μm. The other two stations include dust over the whole size range.

1119
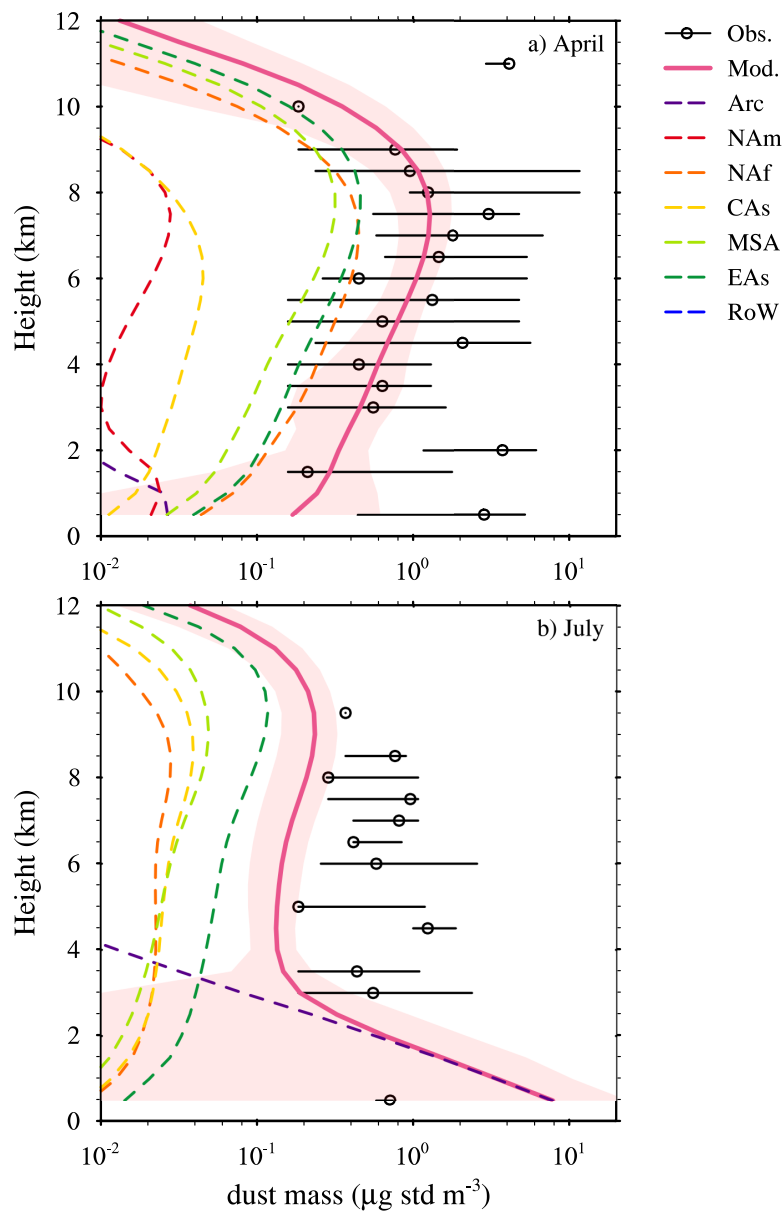
1120

Figure 4. Comparison of vertical dust concentrations from ARCTAS flight observations (Jacob et al., 2010) (black circle) and CTRL simulation (pink solid line) in a) April and b) July. We show median values for observations at each level. The maximum and minimum of the measurements at each level are shown by black lines. Contributions from the seven tagged sources in CTRL are shown by colored dashed lines. The ARCTAS dust mass concentrations are derived from measured calcium and sodium concentrations. The measurements data are processed using the same method as Breider et al. (2020). Briefly, we assume a calcium to dust mass ratio of 6.8% and further correct the calcium concentrations for sea salt by assuming a calcium to sodium ratio of 4%. Only measurements obtained north of 60°N are used for the analyses. The low-altitude observations near Fairbanks, Barrow, and Prudhoe Bay are removed.

1131   Also, data from below 1 km on 1, 4, 5, 9 July is removed to exclude the influence of wildfire.
1132   The ARCTAS flight campaign was conducted in 2008, while the modeled vertical profiles are
1133   averaged for each April and July from 2007 to 2011, respectively. Following Groot Zwaaftink et
1134   al. (2016), the simulation profiles are averaged for the regions north of 60°N and 170°W to
1135   35°W in April and 135°W to 35°W in July. Also, the observations have a cut-off size of 4 μm
1136   and thus is only compared with simulated dust concentrations in the same size range. The pink
1137   shade on each panel represents the standard deviation with respect to time and space for the
1138   simulated total dust concentrations.

1139
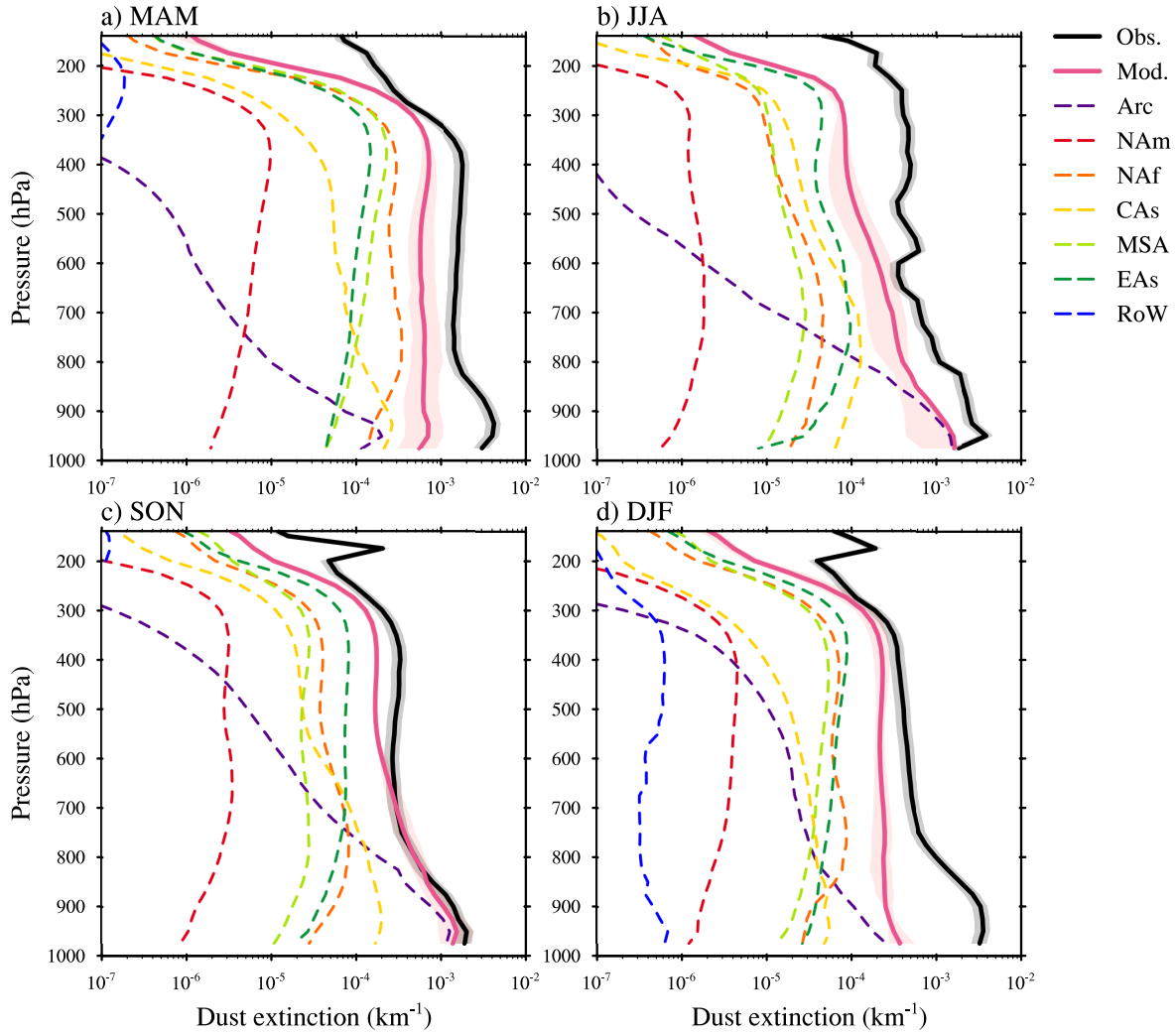
Figure 5. Comparison of seasonal CALIPSO retrieved (Luo et al., 2015a, b; Yang et al., 2022) (black solid line; with gray shade representing uncertainty) and model simulated (pink solid line; with pink shade representing year-to-year variability) dust extinction vertical profiles in the Arctic (above 60°N). Contributions from seven tagged sources are shown by colored dashed lines. The CALIPSO retrievals are for the year 2007 to 2009, while the model results are averaged over the same years. The uncertainties of the CALIPSO retrievals are assumed to be 20% following Yang et al. (2022).
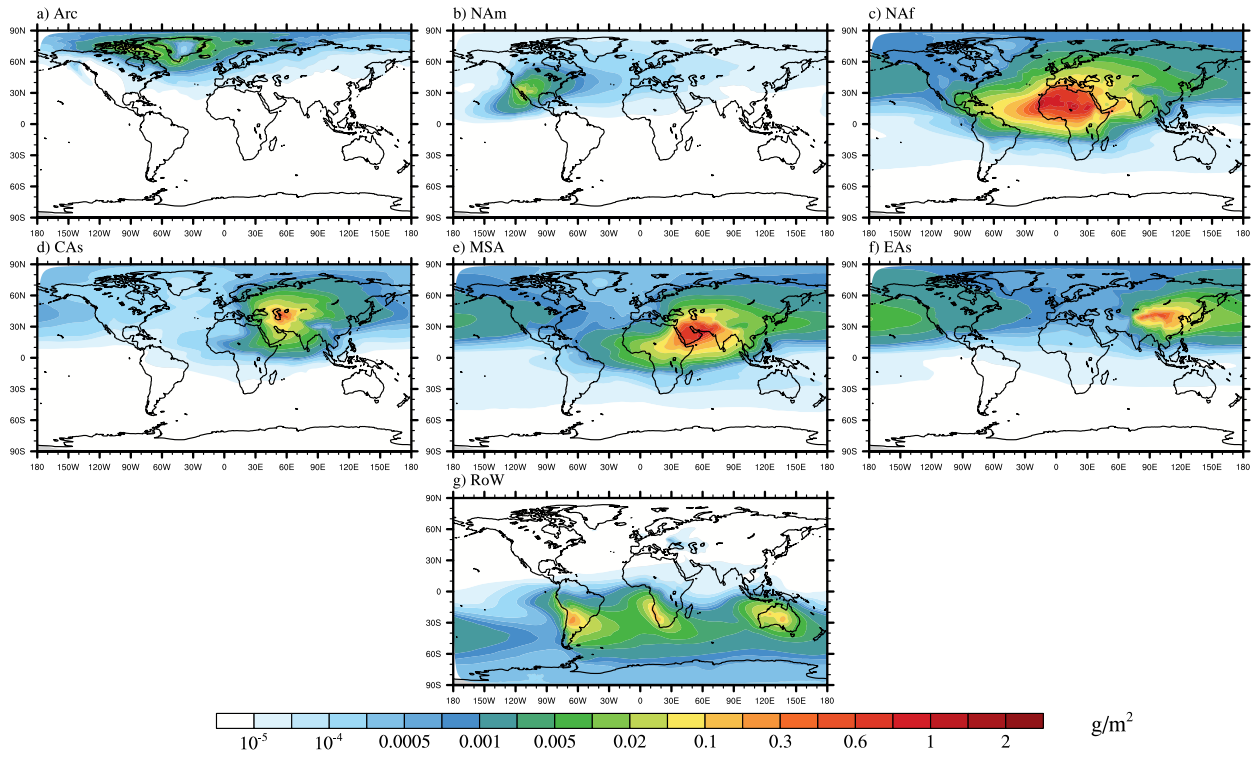
1148

1149   **Figure 6.** Spatial distribution of annual mean (year 2007 to 2011) dust column burdens for
1150   various tagged sources.
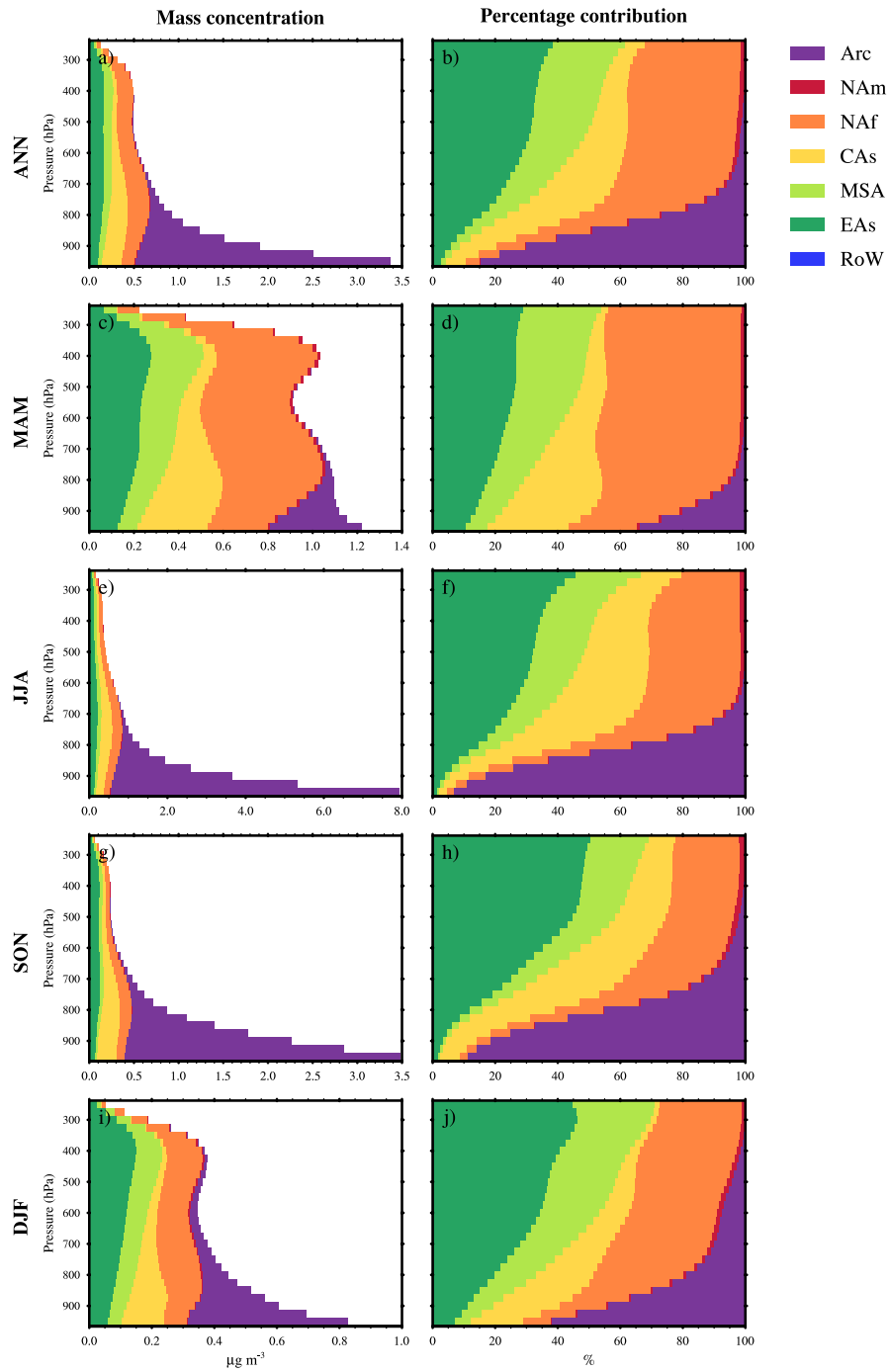
1151

Figure 7. Annual and seasonal mean (year 2007 to 2011) Arctic (60-90°N) vertical dust
concentrations (left panel) and percentage contributions from tagged sources (right panel).
Different tagged sources are classified by different colors.
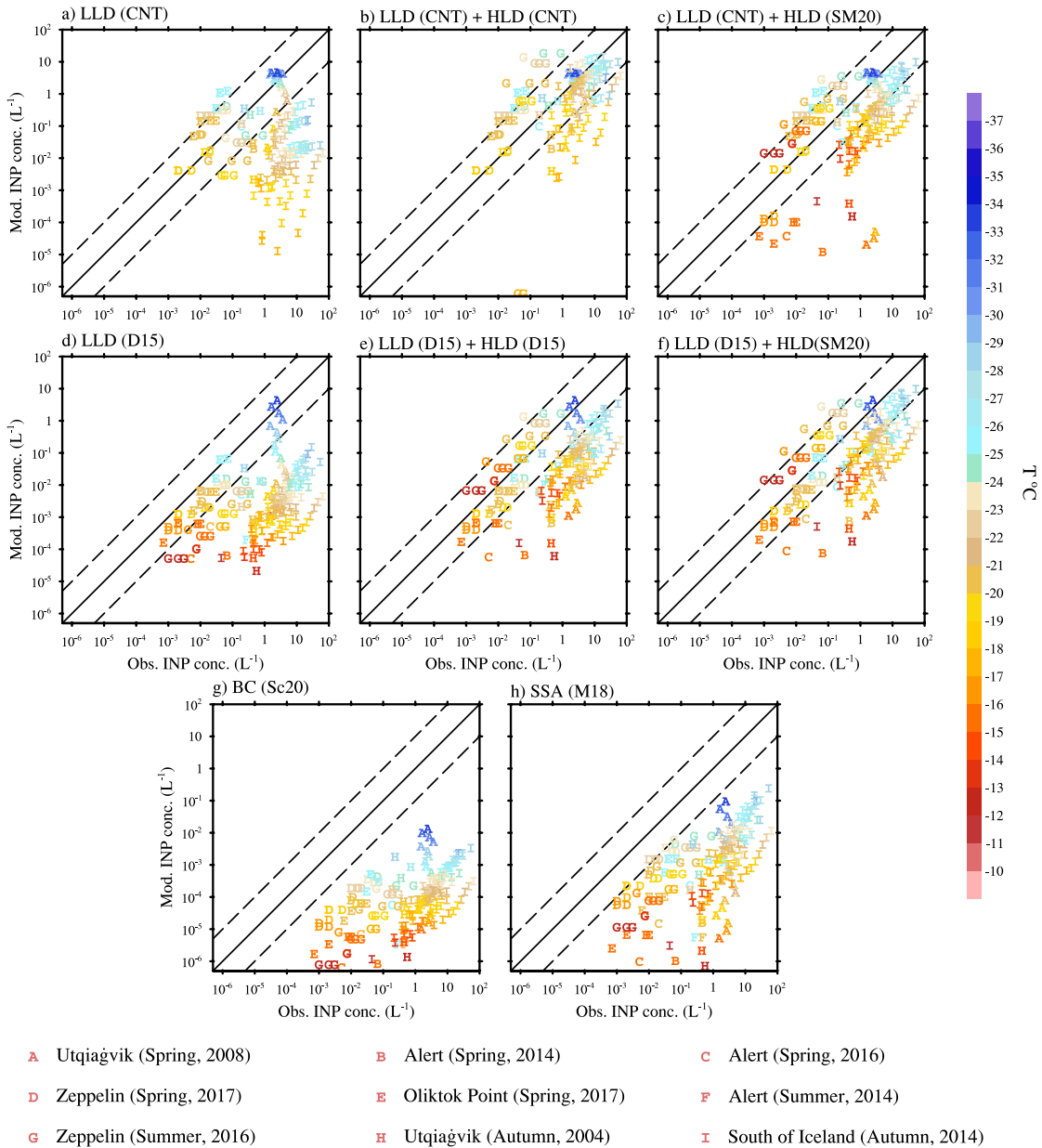
Figure 8. Comparison of predicted versus observed INP concentrations in the Arctic. The predicted INP concentrations are derived from a) LLD using classical nucleation theory (CNT), b) LLD and HLD, both using CNT, c) LLD using CNT and HLD using Sanchez-Marroquin et al (2020; SM20), c) LLD using DeMott et al. (2015; D15), d) LLD and HLD, both using D15, e) LLD using D15 and HLD using SM20, f) BC using Schill et al. (2020; Sc20), and g) SSA using McCluskey et al. (2018; M18). SSA includes both marine organic aerosol and sea salt. Nine INP datasets are classified by symbol "A" to "I", the color of which represents the temperature reported in the observations. The observations for datasets "A", "C", "E", "H" are monthly mean values. Samples for datasets "D", "G", "I" are selected randomly and only 15% of them are plotted. Details of each campaign are summarized in Table 3. The modelled INP concentrations

1166   are diagnosed using the observed temperatures and monthly averaged aerosol properties of the
1167   corresponding month from year 2007 to 2011. The INP concentrations for CNT are defined as
1168   the CNT immersion freezing rate integrated by 10 s, following Hoose et al. (2010) and Wang et
1169   al. (2014). Solid line in each panel represents 1:1 comparison, while dashed lines outline one
1170   order of magnitude differences. The unit for INP concentration is L^{-1}.

1171
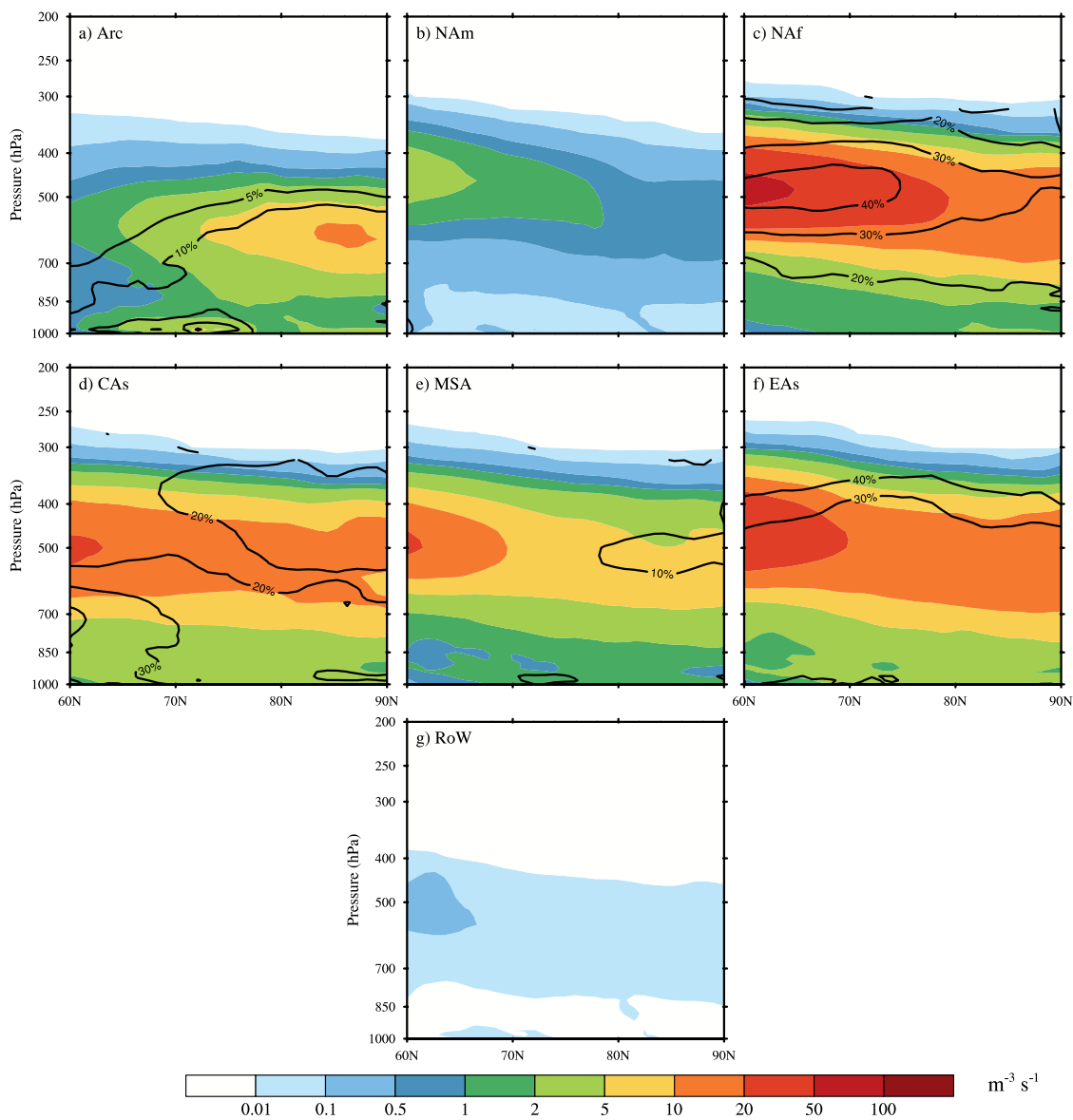
1172

Figure 9. Annual and zonal mean (year 2007 to 2011) ambient mixed-phase cloud immersion freezing rates (unit: m^{-3} s^{-1}) in the Arctic for the seven dust sources. Black contours are the percentage contributions from each dust source to the total immersion freezing rate.

1173
1174
1175

1176
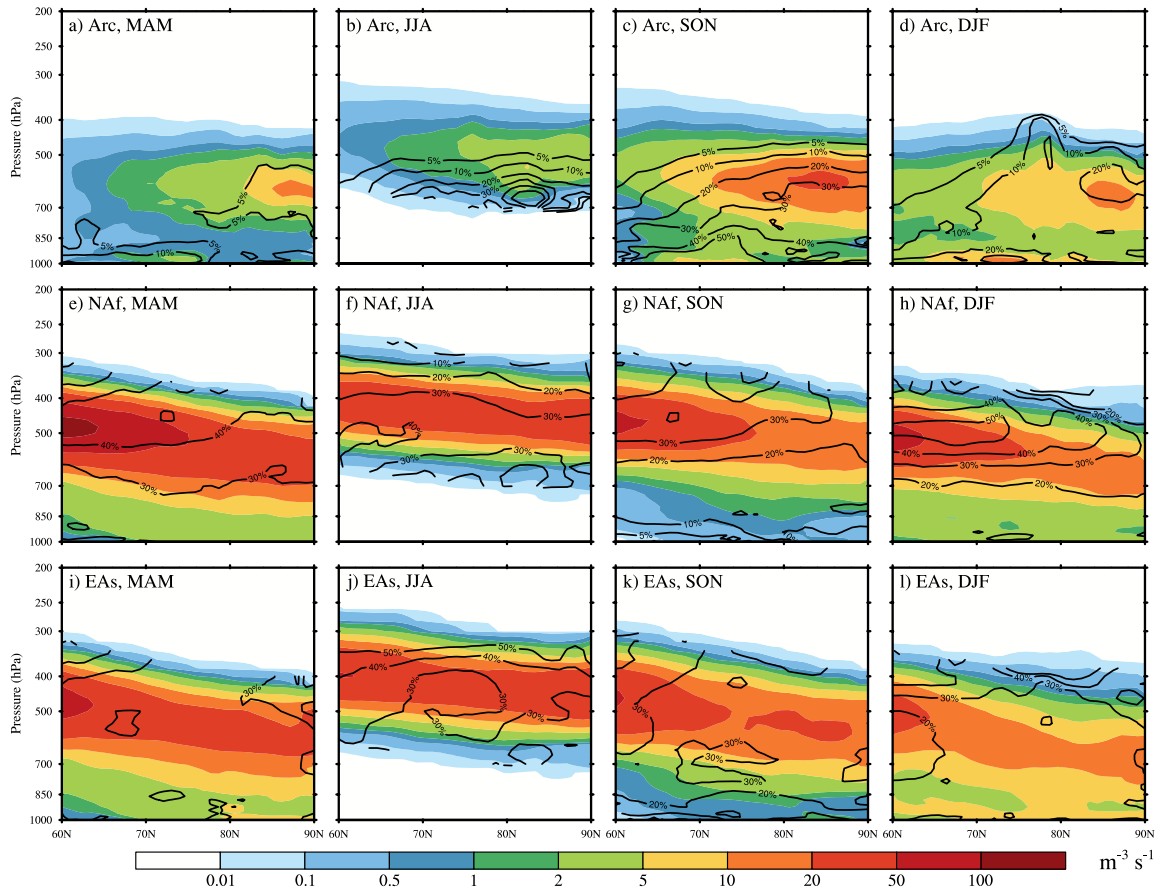
Figure 10. Seasonal variations (year 2007 to 2011) of the mixed-phase clouds immersion freezing rates (unit: $m^{-3} s^{-1}$) over the Arctic for dust emitted from the Arctic (top panel), North Africa (middle panel), and East Asia (bottom panel). Black contours are the percentage contributions from each dust source to the total immersion freezing rate in the corresponding season.
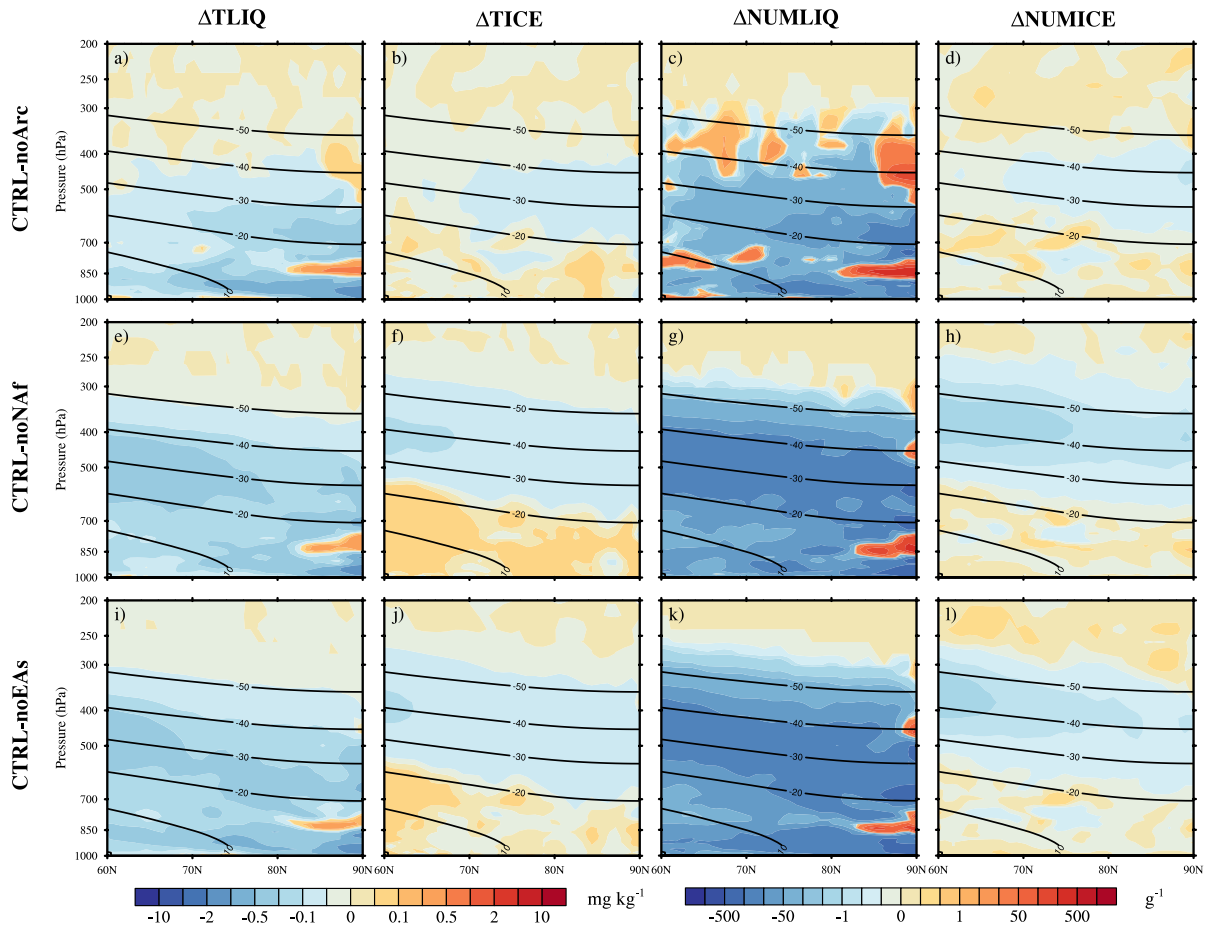
1184

Figure 11. Annual and zonal mean differences (year 2007 to 2011) in total liquid water mass mixing ratio (TLIQ), total ice mixing ratio (TICE), cloud droplet number concentration (NUMLIQ), and cloud ice number concentration (NUMICE) in the Arctic. Black contours are zonal averaged temperatures in °C. Top, middle, and bottom panels show the differences between CTRL and noArc, noNAf, and noEAs, respectively.
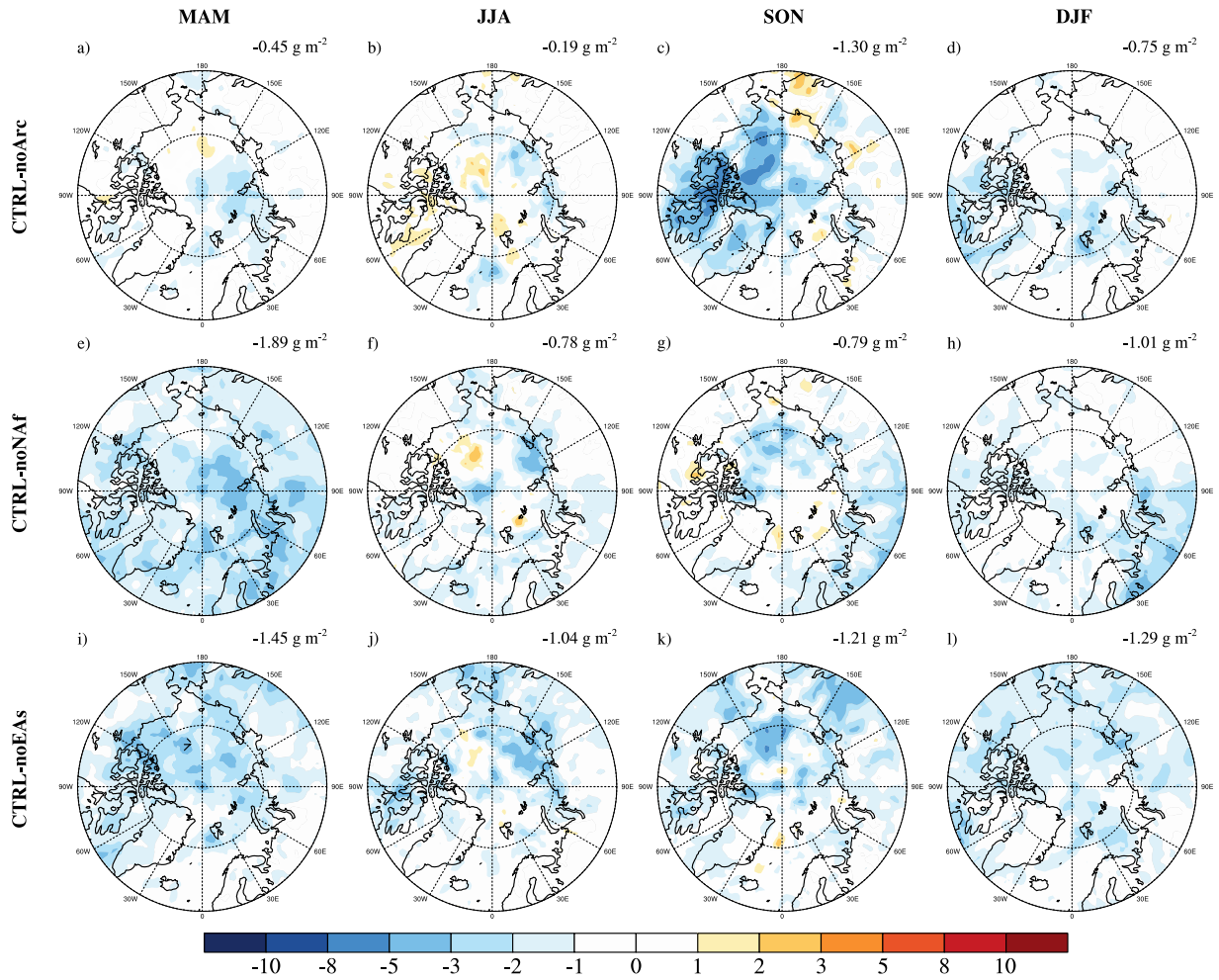
1190

Figure 12. Seasonal changes (year 2007 to 2011) in LWP (unit: g m^{-2}) caused by dust INPs from the Arctic (top panel), North Africa (middle panel), and East Asia (bottom panel). The numbers are averaged LWP differences in the Arctic.

1191
1192
1193

1194
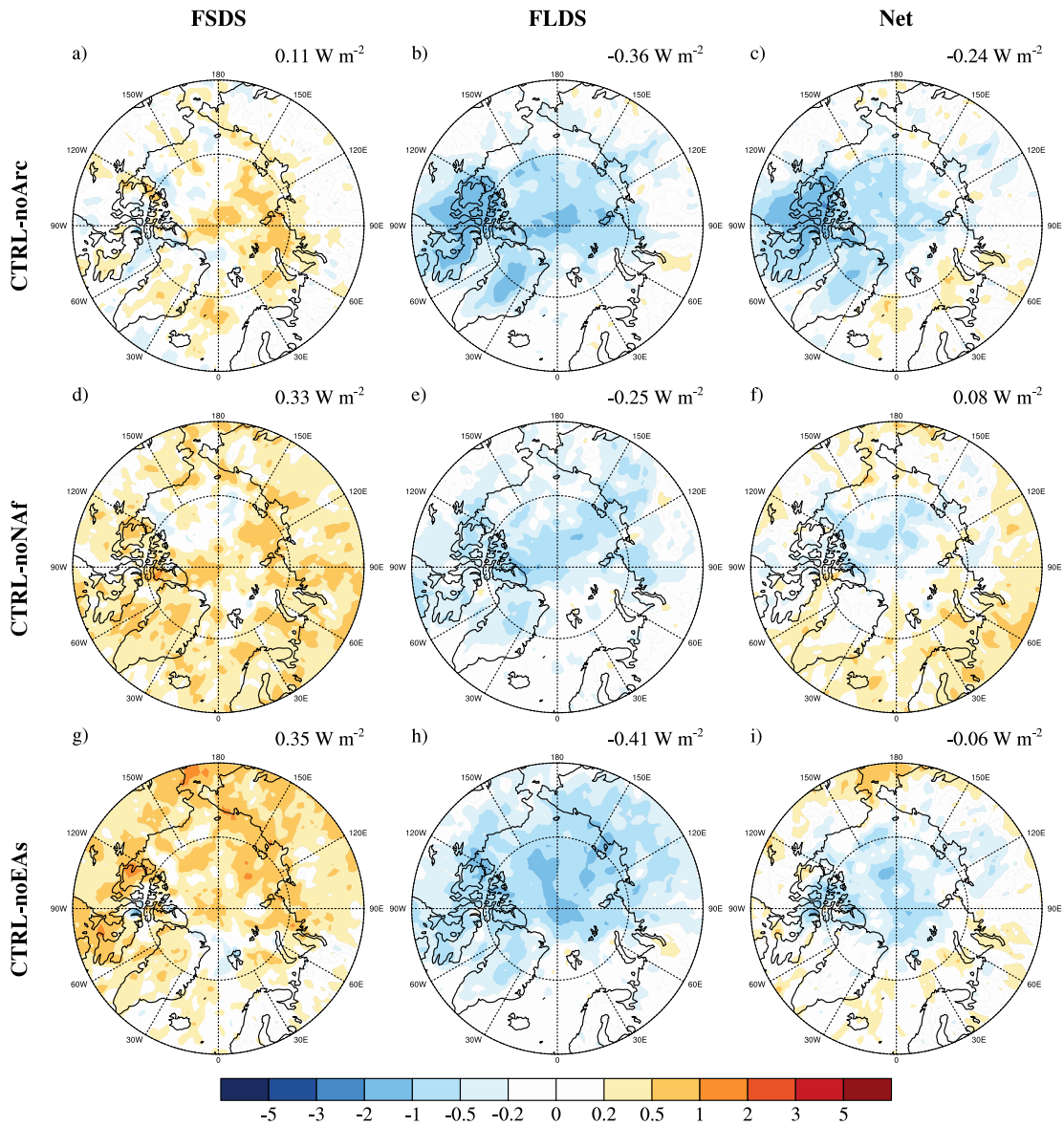
Figure 13. Changes in annual mean (year 2007 to 2011) downwelling radiative fluxes at the surface (unit: W m^{-2}) caused by dust INPs from the Arctic (top panel), North Africa (middle panel), and East Asia (bottom panel). Left, middle, and right panels are downwelling shortwave (FSDS), longwave (FLDS), and net (FSDS + FLDS) radiative fluxes, respectively. The numbers are averaged radiative flux differences in the Arctic.
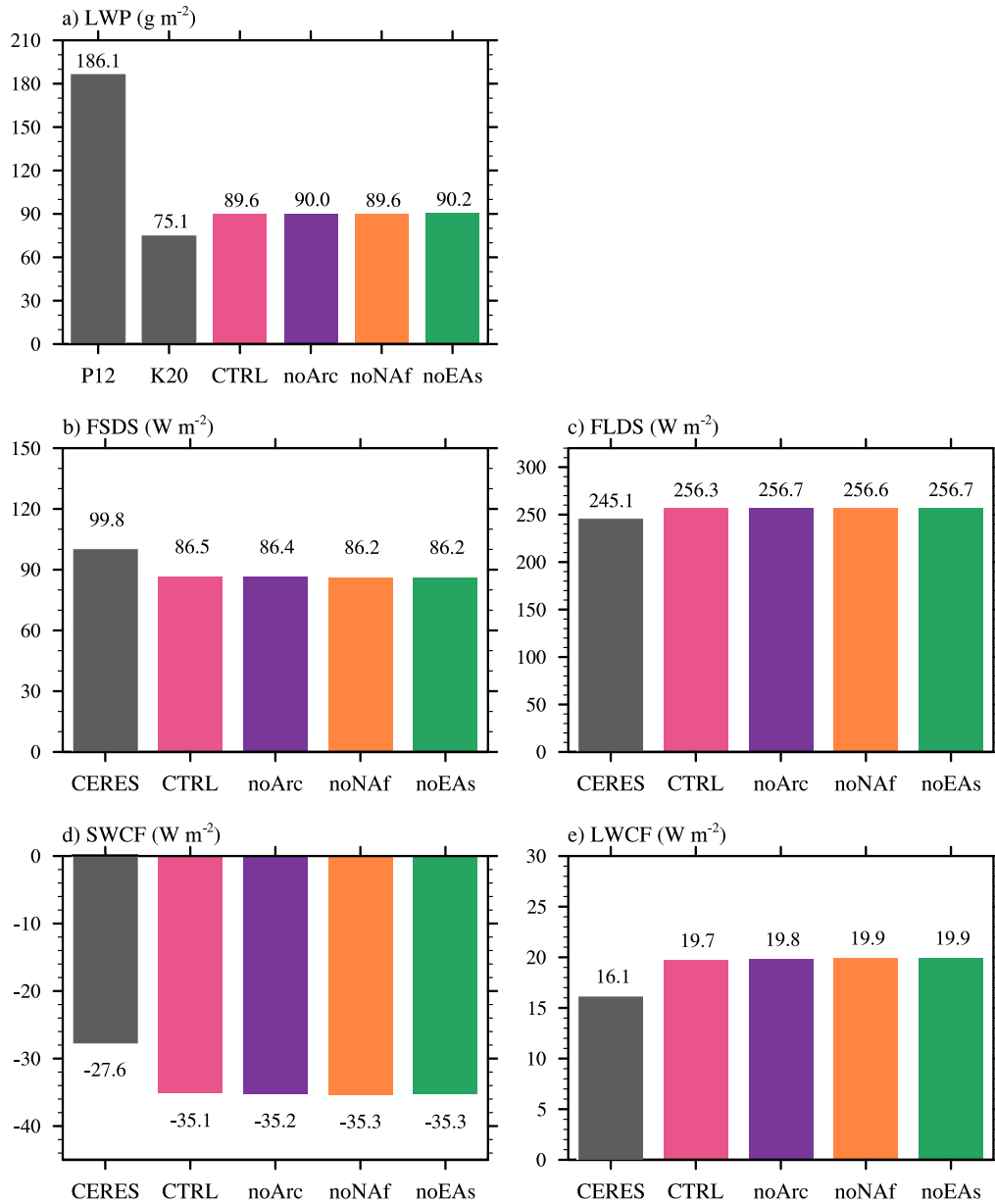
Figure 14. a) Annual mean Arctic (60°N to 80°N in this subplot) averaged LWP over ocean for the MODIS observations and the four simulations (2007-2008). Two MODIS datasets are used, including the standard product (Pincus et al., 2012; P12; averaged from 2007 to 2008) and an improved one (Khanal et al., 2020; K20; averaged from 2007 to 2009). The MODIS simulator is used to calculate the simulated LWP. b) - e) Annual mean Arctic (60°N to 90°N in these subplots) averaged b) FSDS, c) FLDS, d) SWCF, and e) LWCF for the CERES observation (2007-2011) and the four simulations (2007-2011).